



HAL
open science

Geophysical and hydrogeological investigations of water leakage from a reservoir dam to a coastal aquifer: the Lebna Case Study (Northeastern Tunisia)

Nejmeddine Ouhichi, Radhouane Hamdi, Fethi Lachaal, Hakim Gabtni,
Olivier Grünberger

► To cite this version:

Nejmeddine Ouhichi, Radhouane Hamdi, Fethi Lachaal, Hakim Gabtni, Olivier Grünberger. Geophysical and hydrogeological investigations of water leakage from a reservoir dam to a coastal aquifer: the Lebna Case Study (Northeastern Tunisia). *Arabian Journal of Geosciences*, Springer, 2022, 15 (13), pp.1192. 10.1007/s12517-022-10318-9 . hal-03709374

HAL Id: hal-03709374

<https://hal.archives-ouvertes.fr/hal-03709374>

Submitted on 29 Jun 2022

HAL is a multi-disciplinary open access archive for the deposit and dissemination of scientific research documents, whether they are published or not. The documents may come from teaching and research institutions in France or abroad, or from public or private research centers.

L'archive ouverte pluridisciplinaire **HAL**, est destinée au dépôt et à la diffusion de documents scientifiques de niveau recherche, publiés ou non, émanant des établissements d'enseignement et de recherche français ou étrangers, des laboratoires publics ou privés.

Geophysical and Hydrogeological Investigations of Water Leakage from a Reservoir Dam to a Coastal Aquifer: The Lebna Case Study (Northeastern Tunisia)

Nejmeddine Ouhich ^{1,2,3,*}, Radhouane Hamdi ³, Fethi Lachaal ¹, Hakim Gabtni ¹, and Olivier Grunberger³

¹ LGR/LR15 WRTC 01, CERTE, Borj Cedria Ecopark, Soliman, Tunisia

² FST, Campus Universities, El Manar, Tunis, Tunisia

³ Univ Montpellier, INRAE, IRD, Institut d'Agro, UMR LISAH, Montpellier, France

Corresponding Author: nejmeddinouhichi@gmail.com

Abstract

In semiarid regions, dams are useful for surface water storage, sediment sequestration, and aquifer recharge. Built in 1987 on the Cap Bon peninsula (in northeastern Tunisia), the Lebna Dam is considered a good example of a multifunctional reservoir. The dam feeds two important irrigation networks, stores large sediment quantities, and allows a significant recharge flow to the underlying aquifer.

This work suggests new leakage flow and dam-aquifer interaction characterizations through the development of an approach that combines a water balance calculation, geological field observations, groundwater monitoring, and geophysical research.

The hydrological balance calculation performed over the monitoring period (1990-2017), shows that an estimated water volume of $3.7 \text{ Mm}^3 \text{y}^{-1}$ has leaked from the Lebna reservoir to the coastal aquifer. Geological mapping of the Lebna Dam basin in summer 2019 revealed the existence of permeable layers of sands to sandstones exposed along the southern banks of the reservoir and extending to an elevation that included the water level when the dam is full; these rocks outcrop at approximately 16 m.a.s.l.

A geophysical survey based on 67 vertical electrical soundings and 8 electrical resistivity tomography profiles in the area downstream of the reservoir was carried out to identify the

lateral continuity of the recharge zones. Piezometric campaigns consisting of four field surveys in 2019 and 2020 were conducted in the region downstream of Lebna Dam, consisting of 71 water well samples.

The collected evidence led to the conclusion that concentrated recharge occurs in the downstream bank of the dam.

Keywords: Recharge, surface water-groundwater interaction, hydrological balance, resistivity, Electrical conductivity, semiarid zone

1. INTRODUCTION

In Mediterranean countries, dams play a key role in development. Dams are generally built to provide supplementary water that can satisfy the needs of the population, mainly including urban, water flood control and rural irrigation demands. Dams favor the regulation of the hydrologic regimes of rivers and retain sediments (Altinbilek 2002). Nevertheless, they may also cause considerable water losses by evaporation, thereby increasing the salinity of the impounded water and lowering the volume of available water needed for groundwater recharge and alternative uses. Simultaneously, such structures, in turn, may promote the recharge of aquifers. According to de Vries and Simmers (2002), the aquifer recharge is achieved via two key processes: the direct infiltration of precipitation through the soil in outcrop areas and the localized recharge arising from surface water accumulation and sideways percolation (as is the case in this study).

Localized recharge in reservoir lakes depends on various processes and mechanisms (Simmers 1998), and several authors have considered this process to be an indirect supply process (Nazoumou 2002). Thus, recharge can occur in natural lakes or be caused by dams. Therefore, the recharge process relies on many different phenomena, such as dam releases, infiltration wells, and irrigation returns. Leakage through geological embankments that enclose reservoirs can add to silting and evaporation and may result in considerably high water losses (Mesney 2004) and pose severe threats to the stability and security of dam structures (Benfetta et al. 2017). The natural recharge by dams is disrupted in some way by climate change which is increasing from year to year and has short and long-term negative effects on surface water and groundwater in the northern part of the African continent. Since among these consequences the irregularity of precipitation, water degradation, stagnation of

sludge in dams, dead slice, drought, and increased extraction of groundwater, etc. (Hamed et al. 2018)

Leaks occur through materials geological boundaries with a degree of porosity, permeability or discontinuity sufficient to allow the occurrence of water movement (Kim 2013). Leakage is considered a negative effect when it promotes the instability of a dike and/or a significant loss of water; however, leakage can also be considered a positive effect when a nearby aquifer is recharged. The amount of available research on this subject is limited, but examples of reservoir leaks, such as leaks in the such as the Negratín Dam (Spain), Gauting (China), Karoun (Lebanon), and Conqueyrac (France), were cited by Benfetta et al. (2017). Recent works have focused on studying dam leakage processes by quantifying, qualifying or even spatially and temporally delimiting leakage terms (Al-Fares 2011; Berhane et al. 2017; Berhane et al. 2013; Gutiérrez et al. 2015; Kim 2013; Kim and Park 2014; Metwaly et al. 2006; Sevil et al. 2017). Research on the processes associated with leakage through geologic barriers or natural banks is complex due to limited knowledge of the geometry and properties of subsurface rocks. Moreover, because different causes cause leakage in different dams (Benfetta et al. 2017), methods must be adapted to the target case study.

Various techniques have been used to study leakage water entering the boundaries of lakes or dams. Some authors have used isotopic tracers (Alazard 2013; Grünberger et al. 2004; Yi et al. 2018) to detect the contribution of lake water to underground water. Leakage estimates have been computed using surface water budgets, Darcy's law or even by correlating reservoir lake levels with underground water piezometric levels (Bouteffeha, Dages, Bouhlila, & Molenat, 2015). Likewise, researchers have used geophysical techniques such as vertical

electrical sounding (VES) or electrical tomography (Bièvre et al. 2018) to study flow path extents and to delineate leakage areas.

In Tunisia, the government constructed numerous small earthen reservoirs for irrigation, artificial groundwater recharge, and sediment retention. According to the “*General Direction of Dams and Large Hydraulic Works*” (DGBGTH) the state office in charge, numerous dams in the country are suspected to experience leakage (e.g., Beni M'Tir, Kasseb, Barbra, Bou Heurtma, and El Aroussia). Nevertheless, only a few scientific studies have been performed in this region (e.g., Alazard 2013; Dassi et al. 2005). The particular case of the Lebna Dam located in Cap Bon (Tunisia) draws attention. Built to deliver surface water to large coastal irrigation regions to diminish the overpumping of the coastal aquifer (Gaubí et al. 2017; Kerrou et al. 2010), the dam quickly showed evidence of noncontrolled recharge occurring through geological material detected through the modification of piezometric levels. Since its establishment, the Lebna reservoir has never dried up, indicating that the leakage does not endanger the surface water supply. Nevertheless, in light of the available evidence representing this situation, the effectiveness of this recharging system controlled by natural spills in front of an underground salinization region experiencing sea water intrusion is uncertain.

The main objectives of this study are to depict the geological barrier formation by employing fieldwork observations and disclosing the hydrological features of the infiltration processes across the dam bank. To determine the infiltration rate and the ratio between the increase in the Lebna reservoir water level and leakage, data collected from the reservoir were used to characterize groundwater flow through field sampling data. Finally, the aquifer geometry was established, and a surface water-groundwater relationship was defined in the study area.

2. STUDY AREA

The Lebna watershed situated in Tunisia (**Fig. 1a**) has an area of approximately 210 km² and is located in the eastern coastal plain in northeastern Tunisia (**Fig. 1b**). The watershed is bounded on the northwest by the Abdurrahman Mountains, which reach elevations of 650 m.a.s.l, to the northwest by the town of Menzel Temime, to the southwest by the town of Tafelloune, and to the southeast by a slightly marked relief, occupied mainly by annual crops and orchards at elevations close to sea level (**Fig. 1c**).

[Insert Figure 1]

In the southern part of the Lebna watershed, a dam was built at the junction of the El Ouedyenne and Bou Dokhane rivers. The Lebna Dam is the largest constructed dam in Cap Bon; it has an area of approximately 2.822 km², and its capacity is almost 30.4 Mm³; its average yearly water supply reaches 20 Mm³.

As in many coastal regions, overpumping has caused the water table to be overexploited, thus leading to marine intrusion even before dam construction (Kerrou et al. 2010). Several studies have aimed to detect, delineate, or even model this marine intrusion affecting the Korba coastal aquifer. Some of these works include Ziadi et al. (2019), Ziadi et al. (2017), Kerrou et al. (2010), Kouzana et al. (2009), Kouzana et al. (2010), Zghibi et al. (2014); Zghibi et al. (2013); Zghibi et al. (2011), and Paniconi et al. (2001).

3 MATERIALS AND METHODS

3.1 Hydrological Balance

Surface water balance (Thornthwaite and Mather 1957) methods are not frequently used because, at the end, the recharge rate is considered to be equal to the difference between the terms characterizing the decrease in the reservoir volume and evaporation effects, and these terms are often uncertain. However, in our case, this method can lead to satisfactory results, as we have a well-calibrated station on the Lebna dam site at which regular measurements are taken.

In this study, the determination of the hydrological balance of the Lebna Dam is based on the daily water volume conservation method (Albergel et al. 1997). This calculation must consider all the water inputs and outputs from the reservoir (Bouteffeha et al. 2015; Hatch et al. 2010; Schmadel et al. 2014). Data on precipitation, evaporation, pumping, dike leakage, spilling, draining, and pumping for the National Water Supply and Distribution Company (SONEDE) have been collected from the Lebna Dam and used with water level measurements taken in the reservoir to assess the water balance. We assume that when no rain or runoff occurs (most days in the Mediterranean climate), the lake experiences no inflow, and the decreases are explained only by evaporation, the recharge (or natural leakage) volume through the geological materials, and other withdrawals. Then, an estimate of the daily leakage [$\text{m}^3 \text{day}^{-1}$] can be calculated as follows:

$$V_{\text{leak}} = \Delta V - V_{\text{ev}} - [V_{\text{spill}} + V_{\text{Pump}} + V_{\text{SONEDE}} + V_{\text{gate}} + V_{\text{Seepage}}] \quad [1]$$

Where:

ΔV is the stock variation in the dam reservoir from day n to day $n+1$ during a dry period [$\text{m}^3 \text{day}^{-1}$];

V_{ev} is the volume of water evaporated from the reservoir surface [$\text{m}^3 \text{day}^{-1}$];

V_{spill} is the volume of water passing over the spillway (when the reservoir is full) [$\text{m}^3 \text{day}^{-1}$];

V_{Pump} is the volume of water directly pumped for irrigation [$\text{m}^3 \text{day}^{-1}$];

V_{SONEDE} is the volume of water pumped by the National Water Supply and Distribution Company [$\text{m}^3 \text{ day}^{-1}$];

V_{Leak} is the daily subsurface exchange volume from the dam reservoir to the aquifer (dam reservoir-groundwater interaction) [$\text{m}^3 \text{ day}^{-1}$];

V_{gate} is the output drainage volume [$\text{m}^3 \text{ day}^{-1}$] (the dam operator prepares for floods by opening the outlet gate to prevent the spillway from working); and

V_{seepage} is the seepage volume [$\text{m}^3 \text{ day}^{-1}$] under the dam's dike. This value is computed as a power law fitted on a reserved flow plume and as a function of the water body change in the reservoir as follows:

$$V_{\text{seepage}} = 86400 * (Q_{\text{day}(n+1)} + Q_{\text{day}(n)}) / 2 \quad [2]$$

$$Q = a \cdot Wl^b$$

where a is equal to 0.00196702780619;

b is equal to 1.06336220122;

T indicates time;

Q indicates the operating flow rate ($\text{m}^3 \cdot \text{s}^{-1}$); and

Wl is the water level in cm.

All the variables available for observation were measured during the period from 1990 to 2018 (V , V_E , V_{spill} , V_{Pump} , V_{SONEDE} , V_{gate} , and V_{Seepage}). Rainfall data were used only to determine dry periods. The rainfall records were obtained from a rain gauge located at the dam site.

Two slug tests were performed in the two rivers, El Ouedyenne and Bou Dokhane, at the entrance of the reservoir dam to assess the permeability and the water exchanges between the rivers and groundwater upstream of the Lebna reservoir.

Water balance assessments can be applied on different scales depending on the target resolution. For the Lebna Dam, analysis of the water balance process begins using daily water level measurements (**ESM_1.a**). According to the objective of estimating leakage from Lebna reservoir, only dry-season periods were selected, and the daily negative balance values were maintained (**ESM_2.b**). Due to the difference in scale between the water level measurements (measured on a centimeter scale) and the estimated infiltration corresponding to a few millimeters, it was necessary to conduct several aggregations at 5-, 10-, 15- and 20-day intervals. The balance terms were calculated in the same way. However, the value assigned to the date represented a sum of the 5-, 10-, 15- or 20-day increments. From the water level graph derived as a function of time at the chosen interval (**ESM_1.c**), we classified years, according to the water level intervals, into eight groups (**Tab.1**). Each group was assigned an instantaneous average water level value attributed to an average infiltration rate. May, June, July and August represent the recession period. When estimating the infiltrated water volume, this period is preferred. The infiltration volume was estimated according to the surface area of the Lebna watershed.

[Insert Table 1]

3.2 Geological Survey

To complement the existing geological maps, a field mapping survey of the Lebna Basin was performed in August 2019 at a scale of 1:10000 to determine the levels permitting natural

leakage from the Lebna Dam. The survey was based on previous regional works regarding sedimentary deposits in the Cap Bon region (northeastern Tunisia) and included sedimentological aspects (Colleuil 1976; Ben Salem 1992), biostratigraphic aspects (Hooybergs 1995), tectonic aspects (Salem 1992) and stratigraphic and biostratigraphic continuity aspects up to the Hammamet region (Temani et al. 2016). Detailed observations were performed on dam bank outcrops and of two series in quarry pit facies (Q1 and Q2) located at approximately 300 and 600 m from the reservoir ridge, respectively, representing useful outcrops for cartography and calibration.

3.3 Applied Geophysical Survey

3.3.1 Vertical Electrical Sounding VES

The VES surveys describing vertical variations in the apparent electrical resistivity of geological formations (Samouëlian et al. 2005) were performed in April 2019 at 68 sites in the study zone (**Fig. 1b**) using the Schlumberger electrode configuration, which is less time consuming and provides the subsurface geologic layers at a higher resolution compared to the other configurations (Loke et al. 2003). The acquisition was performed using an ABEM TERRAMET~R SAS 4000 along the downstream part of the Lebna reservoir body. The principal objective was to determine the extent of leakage through the geological bank, obtain a global idea of the extension of the recharge zone, and define the geometrical structure of the region downstream of the dam. The AB length extended up to 150 m and reached 300 m in some VES regions during data acquisition, depending on field access.

The determination of layers' thicknesses and resistivity is manually obtained by relating the VES field curves to the theoretical master curves and auxiliary point charts. The interpretation has been carried out confronting the 1D inversion technique software (IPI2WIN, Russia) and

the WINSEV program (Jenny and Borreguerro 1993). An example of the VES treatment is shown on (ESM_2)

3.3.2 Electrical Resistivity Tomography (ERT)

Geophysical investigations were conducted using ERT profiles at two sites on the downstream edge of the reservoir (**Fig. 1b**). The locations of these profiles were chosen in the vicinity of the recharge input zone and according to the monitoring wells available for calibration purposes. A grid of four profiles was formed at each of the two sites. A Wenner-alpha array with 10-m spacing between electrodes was constructed to collect the resistivity data, reaching an investigation depth of approximately 70 m. The electrical resistivity tomography data are presented in the form of inverted resistivity model including topography obtained using Res2DINV Software. The inversion algorithm is based on the standard smoothness-constrained least-squares inversion algorithm (Gauss–Newton method) (De Groot-Hedlin and Constable, 1990; Sasaki, 1992). For all models, the root mean square (RMS) error of the inversion in the resistivity model is less than 5%, which is well acceptable and the models are tolerable (ABEM, 2010)

3.4 Piezometry and Water Quality

Knowledge of piezometric data is of sharp interest when assessing groundwater flow directions and identifying aquifer recharge zones (Chenini et al. 2010).

Four piezometric field campaigns were conducted in the Lebna Basin region in the wet (February) and dry (August) seasons of two successive years, 2019 and 2020. Phreatic groundwater levels were measured in 71 available wells distributed in the study zone (**Fig. 1b**). The resulting isopiezometric lines were interpolated with the kriging method using Surfer 14 software (Golden Software, Golden, CO, USA). The water table piezometric level represented on maps was measured relative to sea level (meters above sea level: m.a.s.l) based

on data obtained in the Shuttle Radar Topography Mission (SRTM), on a differential global positioning system (DGPS) survey conducted at some points and from a 1:25000 topographic map of the region. The relations between groundwater and the Lebna reservoir were considered in the interpolation. The dam water level was considered a piezometric level representing the reservoir shoreline.

For the water quality electrical conductivity measurements, 71 wells were monitored over the same periods. This monitoring campaign also concerned the Lebna Dam water, and the resulting data were used to produce spatialized maps to delimit areas affected by the groundwater recharge induced by the impoundment of the dam.

4 RESULTS

4.1 Lebna Basin Lithological Description

Since 1971, numerous investigations have been conducted in this area, including geological surveys, drilling, geological logging, permeability tests, and geophysical investigations. Specifically, many authors have conducted detailed reviews of the geology of the Cap Bon and Korba regions (Abdeljaouad et al. 1998; Ennabli 1980; Hooyberghs 1995; Ben Salem, 1992, 1995). We focused our research essentially on the Lebna Dam and its downstream section (**Fig. 1b**). The formations outcropping in the study area include Mio-Plio-Quaternary deposits (Ben Salem, 1998). The lower part of the middle Miocene deposits corresponds to detrital deposits, while the upper part is composed of lenticular sandstones and marls with some lignite levels, referred to as the Saouaf Formation. In the study area, deposits from the Upper Miocene are missing due to the widespread erosion that occurred during the Miocene orogeny (Ennabli 1980). Transgressional marine Pliocene sediments cover unconforming

older folded and eroded formations and constitute the main aquifer corresponding to Astian sandstone sediments, called the Porto Farina Formation. These deposits are mainly composed of sandstone, sand, and marl alternations topped by sandstones and sands (Derbel et al., 1991). This lithology changes laterally to contain argillaceous sands or consolidated sandstones that are more or less argillaceous. Pliocene formations largely outcrop in the northern reach of the Lebna River but are completely covered by Quaternary deposits in the Tafelloune and Diar El Hajjej areas (Ennabli, 1980). These Quaternary deposits are composed of two units. The lower marine facies unit corresponds to sandy limestones containing mollusks. The upper unit is composed of continental sediments (Ozer et al. 1980) containing oolitic limestones and coprolites or pelloïdes. These deposits currently form a coastal consolidated wind dune built following marine regression (Chakroun et al. 2005). Old, consolidated dunes cover the Tyrrhenian deposits (Ozer et al., 1980), forming an essential feature of the littoral topography of the Cap Bon peninsula. This geological investigation of the study area allowed us to establish a Lebna Basin map series (**Fig. 2**), containing seven units, as follows, from the base to the top (1 to 7):

1. A gypsum gray marl layer;
2. alternating sandstone layers corresponding to a continuity of the Souaf Formation from the upper Miocene, which is thickest in this zone and forms several depositional sequences;
3. a series of 5- to 6-m-thick plastic gray clays, known in the published literature as the Sidi Barka Formation (Colleuil 1976) of the Lower Pliocene; these clays can be considered the floor of the aquifer;
4. upon these clays lies a sedimentary unit with a total thickness of 8 to 10 m, composed of bioclastic sandy levels alternating with lumachelic sandstones and organized in several layers. The base of each layer shows bioclastic sands with fine and

homogeneous granulometry and an ochre-yellow color, some of which contain sandy lenses. The fauna appears to be reduced, showing fragments of lamellibranch valves. This sedimentary unit ends with a very fossiliferous sandstone term containing large Pectinidae and Ostreidae fossils. This stratigraphic unit is known in the literature as the Hammamet Formation consisting of sand and sandstone (Colleuil 1976);

5. the section ends with coarse reddish sand that becomes yellowish following breakage and is fine-grained and beige to pink;
6. the latter end contains magnesian limestone crusts that outcrop extensively in the area. These crusts likely correspond to the continental Villafranchian described in the literature; and
7. current alluvium sourced from upstream watersheds during flooding events constitutes the reservoir lake floor.

[Insert Figure 2]

4.2 Water Balance Analysis

A statistical analysis performed at different lag-time intervals allowed the selection of an optimal interval time of 10 days; this lag time showed the lowest dispersion in the leakage estimates. An analysis of the curve plotted after calculations showing the average infiltration versus the dam water level (**Fig. 3**) revealed the following information: the infiltration value rose as the water level increases, and two different slopes exist. One slope was found between the 12.5 and 16-m levels, where infiltration rises very slowly from $0.015 \text{ mm.day}^{-1}$ ($3.6 \times 10^{-5} \text{ m}^3 \cdot \text{s}^{-1}$) to $0.025 \text{ mm.day}^{-1}$ ($6.3 \times 10^{-5} \text{ m}^3 \cdot \text{s}^{-1}$); under these conditions, the contribution of subsurface flow is restricted. A second slope was found in which concentrated recharge

increases at 16 m and reaches a maximum of $0.09 \text{ mm}\cdot\text{day}^{-1}$ ($2.1 \text{ m}^3 \cdot \text{s}^{-1}$) at a water level of 18.04 m.

[Insert Figure 3]

The average effect can be summarized with a curve expression that links the groundwater recharge to the water level in the lake. This expression, applied to the time series of the dam water level, allowed us to estimate a volume of $3.76 \text{ Mm}^3\cdot\text{y}^{-1}$ over a period of 27 years. The examination of the reservoir levels from 1990 to 2017 (**ESM_1a**) showed many periods of water storage and destocking. The water volume stored in the reservoir reflected rapid and frequent increases in February of 1996, 1999, and 2015 and in November of 1999; these increases were related to high rainfall during the corresponding period. Less-frequent flood events occurred in March 2007 and April 2009.

Notably, low annual recharge corresponds to dry years and high annual recharge corresponds to rainy years (**Fig. 4**). Most likely, a linear correlation exists between the total annual rainfall and the annual recharge. As more rainfall occurs, the reservoir is filled, and more recharge is thus generated. However, the infiltration tendency is in accordance with the reservoir filling behavior. Indeed, the maximum infiltration value ($5.65 \text{ Mm}^3\cdot\text{y}^{-1}$) was recorded during the 1999-2000 year, when maximum rainfall occurred, and the minimum infiltration value ($1.6 \text{ Mm}^3\cdot\text{y}^{-1}$) corresponded to 2010-2011, when minimum rainfall occurred. In addition, March, April and May presented the highest dam infiltration values. Based on the infiltration law and by interpolating these values, the infiltrated volume was estimated to be $17.9407 \text{ mm}/\text{year}$ over the entire watershed. The global computed leakage rate represented approximately 16% of the inflow entering the reservoir. This amount was then compared with the evaporation

value of 29.54%. A schematic figure was drawn to visualize each term separately using annual averages (**Fig. 5**).

[Insert Figure 4]

[Insert Figure 5]

4.3 Geophysical Results

4.3.1 Electrical Resistivity Tomography (ERT)

The obtained ERT profiles were inverted to electric tomography resistivity models and highlighted three distinguished zones (**Fig. 6 and 7**). The main objective was to detect the preferential infiltration zones, and the edges of the dam were found to allow more infiltration than the other zones.

[Insert Figure 6]

[Insert Figure 7]

For the first layer, 2 to 3 meters from the surface, resistivity values between approximately 20 and 60 Ω .m were detected, with a clear change from one profile to another due to the topography effect. Some heterogeneity existed due to the presence of the clays or marl beds that had already been mapped around the dam bank. This level was not completely continuous; thus, it was absent in some zones and formed small, convex shapes on some profiles. The second layer showed high resistivity values between 140 and 700 Ω .m, contrasting with the deepest part of the ERT profile records corresponding to the clay bedrock (with resistivity values lower than 20 Ω .m). The described layers had the same order of

resistivity as the highest topographic part of the profiles, although their depths varied. This layer also showed a highly variable thickness.

Lateral changes from high to low resistivity, especially near the surface, may have been caused by discontinuities and/or abrupt facies changes. The integrated interpretation of the data aimed to distinguish among the infiltration zones at the two different investigated sites to identify the zone that was the most susceptible to leakage. The water levels on the day's measurements were taken were well marked on the resistivity profiles. The area above the water level traced on the profiles showed very high resistivity values, belonging to the dam-aquifer contact zone with the sandy sandstone formation of the upper Pliocene. The contact areas permitting aquifer recharge at the first site (site 1) were more frequent than those at the second site (site 2).

4.3.2 Vertical Electrical Soundings (VES) Interpretation

The determination of layers' thicknesses and resistivity is manually obtained by relating the VES field curves to the theoretical master curves and auxiliary point charts. The interpretation has been carried out confronting the 1D inversion technique software (IPI2WIN, Russia) and the WINSEV program (Jenny and Borreguerro 1993). The VES inversion provided an electrical image of the underground structure from the surface up to a depth of 100 m. six maps were selected among 14 maps produced (**ESM_2**). The maps represented the apparent resistivity variation over the whole zone covered by the Lebna Basin along a section of subsoil varying in thickness between 3 and 75 m. The resistivity range denoted on the maps varied between 0 and 700 Ω .m, and high resistivity values [$> 90 \Omega$.m] were concentrated downstream of the reservoir lake. The apparent resistivity showed circular to subcircular shapes ranging from green to red on the scale and indicated either the existence of permeable

layers allowing recharge near the dam or even zones farther away that were convenient for the implementation of water drilling.

In the area near the dam, on the right bank side, the maps show high-resistivity zones ($>70 \Omega.m$) at different AB/2 locations in contact with the reservoir. Consequently, the dam bank is surrounded by high-value contours, allowing water to flow and partly explaining the water exchange with the Korba aquifer.

The existing borehole BH1 allowed the calibration of the proximal VES, S2-5 (**ESM_3**).

However, the available lithological columns are reconstructed from field observations and calibration based also on two quarries pit facies Q1 and Q2. Interpretation of the rest of the VES will be based on the relationship between resistivity and facies obtained from the BH1 calibration providing the necessary data to develop isobaths and isopach maps of the aquifer delivering information on aquifer geometry.

As result, the top isobath map of the shallow aquifer (**Fig. 8.a**) represents deformations that affect the Plio-Quaternary deposits in the study site. This map shows a NE-SW structure located approximately 500 m south of the lake bank, corresponding to a high structure bordered by a lower area ("H2" on the diagram). Faults or monoclines related to the late Quaternary tectonic extension could have generated this structure; these structures could be studied by seismic refraction, as was in the study by Buroillet (1991). The resulting isobath map revealed an important element for consideration: the high structure existing in the subsurface on the southern side of the dam. This structure must also be considered to characterize the hydrogeological system. "H1" and "H2" on the map also denote high structures, but their elevations result from topography effects, as they are located farther upstream with higher inclinations. The isopach map of the shallow aquifer (**Fig. 8.b**) shows that the thickness of the sandy aquifer ranged between 5 and 10 m in large areas but was thicker in certain places. A thick zone was located directly south of the dam, enabling a

preferential flow path toward the SE direction in accordance with the topographic slope toward the sea.

[Insert Figure 8]

4.4 Piezometric and Electrical Conductivity Results

The general behavior of the piezometric levels of free aquifers is mostly related to topographic variations (Chenini et al. 2010). This is the case for the piezometric levels of the sandy aquifer studied herein, the piezometric levels of which are mainly oriented parallel to the seashore. By reviewing piezometric maps of 2020 (**Fig. 9**), we detected a southeast general flow direction exiting the southeast bank of the reservoir. The flow path directions show discrepancies in their general directions that are in accordance with the aquifer geometry heterogeneity determined in previous research. Indeed, the average piezometric gradients range from approximately 3‰ and can drop to inferior levels of 5‰ in areas where the aquifer is particularly thick (>20 m); this trend was observed in all 4 seasons, even in 2019, (ESM_4). Near the sea shore (<2 km distance), piezometric levels below sea level illustrate the influence of overpumping above sea water intrusion, as previously studied by researchers (Kingumbi et al. 2005; Kouzana et al. 2009; Zghibi et al. 2013; Ziadi et al. 2019).

[Insert Figure 9]

The underground mapping of electrical conductivity (EC) (Figure 10, ESM_5) illustrated EC values ranging from 0.4 to 7.5 mS.cm⁻¹. The lowest EC values identified in the groundwater were close to those observed in the dam water: 0.8 mS.cm⁻¹ in winter and 1.3 mS.cm⁻¹ in the dry season. Around the reservoir banks, the ECs were usually within these values up to a distance of 1 km during winter and a distance of 500 m during the dry season. Excluding the

August 2020 situation, the EC values identified at some distances from the reservoir seemed to stabilize between 1.8 and 2.6 mS.cm⁻¹ (corresponding to total dissolved solids (TDS) values of ~0.9 to ~1.3 g/L) in large areas. These values are characteristic of mixing between the reservoir water and underground water, corresponding to a TDS of 2 g/L (EC ~4 mS.cm⁻¹) (Hamouda et al. 2019). In the southeastern part of the study area, the EC values were generally high (> 3.5 mS.cm⁻¹) due to saline intrusion. Similarly, 2 wells in the northwestern part of the study area showed EC measurements greater than 3.5 mS.cm⁻¹ during the 4 seasons sampled (wells W60 & W61). In August 2019, a clear and continuous dilution plume was observed coming from the dam side, while in August 2020, the plume seemed to have been displaced toward the south, as pronounced increases were identified in EC in the wells located at distances between 1 and 2 km from the Lebna Dam.

[Insert Figure 10]

5 DISCUSSIONS

A geological survey was performed to identify and map a sandy formation outcrop known as the Hammamet Formation of upper Pliocene age; this material is present on the southern ridges of the studied reservoir. The position of the formation lies on a layer of Sidi Barka clay (Lower Pliocene), favoring infiltration when water levels are higher than 15 m.a.s.l. The rise of the water level to the dam-dumping height of 18 m.a.s.l should increase at the same time the infiltration surface area and the hydraulic gradient increase. Dam balance calculations indicated that an average water volume of 3.76 Mm³.y⁻¹ +/- 0.02 infiltrated into the water table downstream of the dam throughout the 1990-2017 period, with high variations occurring between wet and dry years. As mentioned by Kerrou et al. (2010) to be coherent with his

modeling of the Korba aquifer, the estimated volume was approximately $3.73 \text{ Mm}^3 \cdot \text{y}^{-1}$ in 2004.

Kerrou et al. (2010) used a unique value as a permanent input to represent the coastal aquifer, whereas we were able to compute varying recharge estimates that could be entered to represent scenarios dedicated to forecasting the evolution of saline intrusion under climate change conditions. The extension and limits of the aquifer downstream of the reservoir were precisely determined by geophysical means combining VES and ETR methods. Tectonic feature and facies changes influenced the aquifer layer flow paths from the reservoir to the sea; for example, the Hammamet Formation presented large thickness variations with clear piezometric patterns. Areas with large aquifer thicknesses implied low piezometric gradients. This description of the aquifer limits constitutes added value that creates opportunities for the simulation and understanding of the responses of the aquifer to recharge and pumping. From the EC and piezometric evolution data, 4 different areas of interest were discriminated:

- 1- Near the reservoir (0-500 m from the south banks), low EC ($<1.8 \text{ mS} \cdot \text{cm}^{-1}$) and piezometric levels were connected to the corresponding lake levels with low gradients, indicating the direct influence of the recharge zone in the Hammamet Formation.
- 2- Downstream (0.5-1 km), tectonic structures narrow the flow paths, and a higher-gradient zone is found with higher EC values [1.8 to $2.6 \text{ mS} \cdot \text{cm}^{-1}$]. The salinity in this region is typical of mixing between underground water and reservoir water
- 3- Downstream (1-2 km), a thicker aquifer zone with low piezometric gradients and similar EC values can be found.

- 4- At approximately the sea shoreline (distance < 3 km), the piezometric gradients are disturbed, and the EC values are elevated ($>2.6 \text{ mS.cm}^{-1}$), indicating overpumping and salt intrusion.

A combination of VES and ERT techniques was used in this study, but as Kayode, Odukoya, Adagunodo, and Adeniji (2018) they found that a combination of seismic refraction and resistivity methods is adequate for obtaining robust information regarding seepage pathways in and around dams. Similarly, the self-potential (SP) and induced polarization (IP) methods are known to be sound for monitoring subsurface seepage (Panthulu et al. 2001); thus, we considered applying these methods in the future near the lake zone, but these methods may be inadequate for sites with piezometric levels deeper than 4 to 8 meters. In this study, the geophysical campaign was carried out during the dry season. It is always possible to perform regular follow-up measurements at different times to detect the resistivity variations on the banks of the Lebna reservoir.

The uncertainties in our piezometric maps are difficult to reduce; few points were measured by DGPS methods (9 out of 71), and for the rest of the analyzed points, SRTM 90 and topographic map data were used, contributing an accuracy of 2 meters. In our experience incorporating DGPS values with topographic map data, the errors were under 50 cm. Nearly all piezometric data are collected in traditional wells that are very often affected by pumping and/or stand as abandoned wells with suspicious water renewal processes. Pumping for irrigation and water returns were not evaluated in the study. Kerrou et al. (2010) estimated an annual pumping value of 100 mm for irrigated zones. We assumed that this value was insufficient for inducing a large water table perturbation. Nevertheless, we recommend complementary temporal monitoring with a pressure probe to document these effects. In most

previous works that explored the dam leakage phenomenon (Dreybrodt et al. 2002; Zhang et al. 2020; Zhao et al. 2012; Zhou et al. 2021), piezometric data were used as the main evidence. In several cases, the data interpretations were based on punctual measurements recorded downstream of the studied dam and correlated to the water level in the reservoir (Zhou et al. 2021). Whenever piezometric maps were presented in the works mentioned above, they were used to describe the flow in general and not the flow perturbations resulting from leakage flow contributions. This consideration resulted in our study being more focused on the detection of zones under the direct leakage reservoir dam effect.

In this study, a relation between the water level and infiltration was established, and the resulting curve included slope changes that corresponded to the limits of sandy layers located in the reservoir bank, as described by geology field surveys. This fact illustrated that an increase in recharge occurs when the lake water level reaches the level of the sandy formations on the southeastern reservoir ridges. The uncertainty in the estimated infiltration volume, obtained through the calculation of some terms in the balance equation, resulted from the manual centimetric measurement accuracy and the simplified working hypothesis regarding the water budget. In contrast, a leakage-water level relationship was established by García-López et al. (2009) in a karstic system. They evidenced a progressive decrease in leakage rates over a certain threshold level and explained this phenomenon by the progressive “saturation of the rock” (the filling of a hydrogeological compartment via a karstic sinkhole). In this case, the resulting equilibrium between the piezometric level and the water level of the reservoir would explain the decrease in leakage flows. In our case, the reservoir level can be considered a piezometrically imposed limit that conditions recharge through a combination of the nearly impermeable alluvial sediments and highly permeable aquifer levels that are reached when the reservoir water level is higher than 16 m.a.s.l.

Boulton et al. (1998) proposed three spatial scales to represent these interactions: the basin/watershed scale, contact zone scale, and sediment scale; these scales were also considered in this paper. Despite previous studies being conducted at the basin scale (Kouzana et al., 2010; Ziadi et al., 2017), few studies analyzed the recharge evolution over different time periods for dam sites located in basins similar to the Lebna Basin. In addition, most previous research has analyzed surface water-groundwater interactions using single methods rather than combinations of multiple field methods; the use of a combination of methods thus represents the added value of the present work.

6 CONCLUSION

Water leakage should be considered when constructing of hydraulic structures such as dams, reservoirs or artificial lakes. This phenomenon can contribute to the study region either negatively (through water losses or dam breakage) or positively (by contributing to the recharge of the groundwater), as in our case study. Investigating the geological nature of the bank layers prior to construction is a major step that can be taken to determine whether leakage will occur and, if so, the order of magnitude. In cases such as our study, the leakage volume mentioned (17% of the dam inflow) was not as critical as that reported in Somers et al. (2016), who suggested a 49% exchange with the subsurface. Nevertheless, this phenomenon was welcomed, as it represented enhanced contribution to the recharge of an overexploited aquifer affected by marine intrusions.

Recharge through the percolation of dam water into natural beds represents an artificial input source to groundwater in arid areas. The choice of method for estimating recharge must be guided by the research objectives, the data availability and the possibility of acquiring

additional data and the scale of the study area. In this paper, we estimated the groundwater recharge volume over a 27-year period in a Mediterranean catchment area using a water balance approach. Electrical resistivity measurements were applied downstream of the Lebna Dam reservoir to precisely detect the locations where leakage occurred. Based on vertical electrical surveys and tomography, resistivity methods allowed the detection of high-resistivity regions corresponding to leakage areas.

The current findings are very useful for stakeholders, especially, to enhance the importance of the Lebna dam as a source of aquifer recharge for the upstream region. Characterization of the Lebna dam / aquifer relationship, improved by a non-controlled leakage of $3.7 \text{ Mm}^3 \cdot \text{y}^{-1}$ from Lebna dam to upstream aquifer and leakage mapping are calculated and presented for the first time.

The characterizations of water leakage and aquifer (groundwater balance, water level, geometry) are useful for: i) local and national water management authorities (DGRE and CRDA Nabeul), to improve sustainable groundwater management strategy, and ii) groundwater users specially the farms in upstream dam, to identify the depth of drilling and wells to reach the aquifer and to know the available groundwater resource.

ACKNOWLEDGMENT

This work has been supported by the International Laboratory NAILA (<http://lmi-naila.com/>) and ALTOS-PRIMA Project (<https://www.altos-project.org>). Authors are grateful for the Lebna dam authority (DGBGTH) and staff that provided site access and shared their operational data set.

DATA AVAILABILITY

The datasets generated during and/or analyzed during the current study are available from the corresponding author on reasonable request.

CONFLICT OF INTEREST

We are not aware of any conflicts of interest related to this publication.

REFERENCES

- ABEM (2010) Instrument manual terrameter SAS 400 / SAS 1000. ABEM Product 33 0020 26, ABEM printed Matter No 93109 (2010-06-04). ABEM Instrument AB, Allén 1, S-172 66 Sundbyberg Sweden.
- Abdeljaouad S, Bensalah M, Truc G (1998) L'Eocène continental en Afrique du Nord: Essai de corrélations biostratigraphique et paléoclimatique. Impact régional périméditerranéen. Notes du Service Géologique de Tunisie, 64, 85-101.
- Al-Fares W (2011). Contribution of the geophysical methods in characterizing the water leakage in Afamia B dam, Syria. *Journal of Applied Geophysics*, 75(3), 464–471. <https://doi.org/10.1016/j.jappgeo.2011.07.014>
- Alazard M (2013) Etude des relations surface – souterrain du système aquifère d' El Haouareb (Tunisie Centrale) sous contraintes climatiques et anthropiques (PhD thesis). University of Montpellier 2, France.
- Albergel J, Rejeb N (1997) Les lacs collinaires en Tunisie: enjeux, contraintes et perspectives. *Comptes-Rendus de l'Académie d'Agriculture de France*, 83(2), 77-88.
- Altinbilek D (2002) The role of dams in development. *International Journal of Water Resources Development*, 18(1), 9–24. <https://doi.org/10.1080/07900620220121620>
- Benfetta H, Ouadja A, Hocini N (2017) Les fuites d' eau dan s les barrages dans le monde: Quelques exemples algeriens water leaks in dams in the world. *Larhyss Journal*, 31, 195–218.
- Ben Salem H (1992) Contribution à la connaissance de la géologie du Cap Bon: stratigraphie, tectonique et sédimentologie. Contribution to the study of the geology of Cape Bon:

stratigraphy, tectonic and sedimentology.) PhD thesis, Faculty of Sciences of Tunis, Tunisia

- Ben Salem H (1995) Evolution de la péninsule du cap Bon (Tunisie orientale) au cours du Néogène. *Notes Serv. géol. Tunisie*, 61, 73-84.
- Bensalem H (1998) Les formations miocènes post-Saouaf des environs de Nabeul (Cap Bon) et leurs équivalents off shore et en Tunisie sud atlasique. *Notes du Service géologique*, (64), 123-128.
- Berhane G, Amare M, Gebreyohannes T, Walraevens K (2017) Geological and geophysical investigation of water leakage from two micro-dam reservoirs: Implications for future site selection, northern Ethiopia. *Journal of African Earth Sciences*, 129, 82–93.
<https://doi.org/10.1016/j.jafrearsci.2016.12.015>
- Berhane G, Martens K, Al Farrah N, Walraevens K (2013). Water leakage investigation of micro-dam reservoirs in Mesozoic sedimentary sequences in Northern Ethiopia. *Journal of African Earth Sciences*, 79, 98–110.
<https://doi.org/10.1016/j.jafrearsci.2012.10.004>
- Bièvre G, Oxarango L, Günther T, Goutaland D, Massardi M. (2018) Improvement of 2D ERT measurements conducted along a small earth-filled dyke using 3D topographic data and 3D computation of geometric factors. *Journal of Applied Geophysics*, 153, 100–112. <https://doi.org/10.1016/j.jappgeo.2018.04.012>
- Boulton A J, Findlay S, Marmonier P, Stanley E H, Valett H M (1998) The functional significance of the hyporheic zone in streams and rivers. *Annual Review of Ecology and Systematics*, 29(1), 59–81. <https://doi.org/10.1146/annurev.ecolsys.29.1.59>
- Bouteffeha M, Dages C, Bouhlila R, Molenat J (2015) A water balance approach for quantifying subsurface exchange fluxes and associated errors in hill reservoirs in

semiarid regions. *Hydrological Processes*, 29(7), 1861–1872.

<https://doi.org/10.1002/hyp.10308>

Burollet P F (1956) Contribution à l'étude stratigraphique de la Tunisie centrale. *Ann. Mines Géol.*, 18, 350.

Burollet P F (1991) Structures and tectonics of Tunisia. *Tectonophysics*, 195(2-4), 359–369.

[https://doi.org/10.1016/0040-1951\(91\)90221-d](https://doi.org/10.1016/0040-1951(91)90221-d)

Chakroun A, Zaghib-Turki, D, Moigne, A. M, de Lumley, H. (2005) Découverte d'une faune de mammifères du Pléistocène supérieur dans la grotte d'El Geffel (cap Bon, Tunisie). *Comptes Rendus Palevol*, 4(4), 317–325.

<https://doi.org/10.1016/j.crpv.2005.01.004>

Chenini I, Mammou A B, Turki M M, Mercier E (2010) Piezometric levels as possible indicator of aquifer structure: Analysis of the data from Maknassy basin aquifer system (Central Tunisia). *Arabian Journal of Geosciences*, 3(1), 41–47.

<https://doi.org/10.1007/s12517-009-0050-4>

Colleuil B (1976) Etude stratigraphique et néotectonique des formations néogènes et quaternaires de la région Nabeul-Hammamet (Cap-Bon, Tunisie) (Doctoral dissertation, Université de Nice).

Dahlin T (1996) 2D resistivity surveying for environmental and engineering applications.

First Break, 14(7), 275–283. <https://doi.org/10.3997/1365-2397.1996014>

Damak-Derbel F, Zaghib-Turki D, Yaich C (1991) Le Pliocène marin du Cap Bon

(Tunisie): exemple de dépôts gravitaires. *Géologie méditerranéenne*, 18(4), 189-198.

Dassi L, Zouari K, Faye S (2005) Identifying sources of groundwater recharge in the

Merguellil basin (Tunisia) using isotopic methods: Implication of dam reservoir water accounting. *Environmental Geology*, 49(1), 114–123. <https://doi.org/10.1007/s00254-005-0069-0>.

- De Groot-Hedlin C, Constable S (1990) Occam's inversion to generate smooth, two dimensional models from magneto telluric data. *Geophysics* 55:1613–1624.
- DGRE (2005). Phreatiques. Direction Generale des Ressources en Eaux, Tunis, Tunisia.
- de Vries, J. J., & Simmers, I. (2002). Groundwater recharge: An overview of processes and challenges. *Hydrogeology Journal*, 10(1), 5–17. <https://doi.org/10.1007/s10040-001-0171-7>
- Dreybrodt W, Romanov D, Gabrovsek F (2002) Karstification below dam sites: A model of increasing leakage from reservoirs. *Environmental Geology*, 42(5), 518–524. <https://doi.org/10.1007/s00254-001-0514-7>
- Ennabli M (1980) Etude hydrogéologique des aquifères du Nord-Est de la Tunisie pour une gestion intégrée des ressources en eau. Thesis, Nice Univ.
- García-López S, Benavente J, Cruz-Sanjulián J, Olías M (2009) Conjunctive use of water resources as an alternative to a leaky reservoir in a mountainous, semiarid area (Adra River basin, SE Spain). *Hydrogeology Journal*, 17(7), 1779–1790. <https://doi.org/10.1007/s10040-009-0466-7>
- Gaubl I, Chaabani A, Mammou A B, Hamza, M H (2017) A GIS-based soil erosion prediction using the Revised Universal Soil Loss Equation (RUSLE) (Lebna watershed, Cap Bon, Tunisia). *Natural Hazards*, 86(1), 219–239. <https://doi.org/10.1007/s11069-016-2684-3>
- Grünberger O, Montoroi J P, Nasri S (2004) Quantification of water exchange between a hill reservoir and groundwater using hydrological and isotopic modelling (El Gouazine, Tunisia). *Comptes Rendus Geoscience*, 336(16), 1453–1462. <https://doi.org/10.1016/j.crte.2004.08.006>
- Gutiérrez F, Mozafari M, Carbonel D, Gómez R., Raesi E (2015) Leakage problems in dams built on evaporites. The case of La Loteta Dam (NE Spain), a reservoir in a large

- karstic depression generated by interstratal salt dissolution. *Engineering Geology*, 185, 139–154. <https://doi.org/10.1016/j.enggeo.2014.12.009>
- Hamed, Y., Hadji, R., Redhaounia, B., Zighmi, K., Bâali, F., & El Gayar, A. (2018). Climate impact on surface and groundwater in North Africa: a global synthesis of findings and recommendations. *Euro-Mediterranean Journal for Environmental Integration*, 3(1), 1-15.
- Hamouda M F B, Leduc C, Tarhouni J, Zouari K (2019) Origine de la minéralisation dans l'aquifère plio-quadernaire de la côte orientale du cap Bon (Tunisie). *Sécheresse*, 20(1), 78–86. <https://doi.org/10.1684/sec.2009.0161>
- Hatch C E, Fisher A T, Ruehl C R, Stemler G (2010) Spatial and temporal variations in streambed hydraulic conductivity quantified with time-series thermal methods. *Journal of Hydrology*, 389(3-4), 276–288. <https://doi.org/10.1016/j.jhydrol.2010.05.046>
- Hooyberghs H J F (1995) Synthèse sur la stratigraphie de l'Oligocène, Miocène et Pliocène de Tunisie. Notes du Service géologique de Tunisie, 61, 63-72.
- Jenny J. Borreguerro M (1993) WINSEV, programme d'interprétation des sondages électriques verticaux réalisés selon le dispositif Schlumberger. W-Geosoft.
- Kayode O T, Odukoya A M, Adagunodo T A, Adeniji A A. (2018) Monitoring of seepages around dams using geophysical methods: A brief review. *IOP Conference Series: Earth and Environmental Science*, 173, 012026. <https://doi.org/10.1088/1755-1315/173/1/012026>
- Kerrou J, Renard P, Tarhouni J (2010) Status of the Korba groundwater resources (Tunisia): Observations and three-dimensional modelling of seawater intrusion. *Hydrogeology Journal*, 18(5), 1173–1190. <https://doi.org/10.1007/s10040-010-0573-5>

- Kim G B (2013) Assessment of water seepage through a geologic barrier surrounding a large reservoir using groundwater levels, soil condition, and a numerical model. *Environmental Earth Sciences*, 69(6), 2059–2072. <https://doi.org/10.1007/s12665-012-2041-0>
- Kim G B, Park J H (2014) Hydrogeochemical interpretation of water seepage through a geological barrier at a reservoir boundary. *Hydrological Processes*, 28(19), 5065–5080. <https://doi.org/10.1002/hyp.9964>
- Kingumbi A, Besbes M, Bourges J, Garetta P (2005) Évaluation des transferts entre barrage et aquifères par la méthode de bilan d'une retenue en zone semi-aride. Cas d'El Haouareb en Tunisie centrale. *Revue des Sciences de L'eau*, 17(2), 213–225. <https://doi.org/10.7202/705531ar>
- Kouzana L, Benassi R, Mammou A B, Felfoul M S (2010) Geophysical and hydrochemical study of the seawater intrusion in Mediterranean semi arid zones. Case of the Korba coastal aquifer (Cap-Bon, Tunisia). *Journal of African Earth Sciences*, 58(2), 242–254. <https://doi.org/10.1016/j.jafrearsci.2010.03.005>
- Kouzana L, Mammou A B, Felfoul M S (2009) Seawater intrusion and associated processes: Case of the Korba aquifer (Cap-Bon, Tunisia). *Comptes Rendus Geoscience*, 341(1), 21–35. <https://doi.org/10.1016/j.crte.2008.09.008>
- Loke M H, Acworth I, Dahlin T (2003) A comparison of smooth and blocky inversion methods in 2D electrical imaging surveys. *Exploration Geophysics*, 34(3), 182–187. <https://doi.org/10.1071/eg03182>
- MESNEY M (2004) Un grand barrage à haut risque. Saddam dam en Irak. Article revue houille blanche. SHF France

- Metwaly M, Khalil M, Al-Sayed E S, Osman S (2006) A hydrogeophysical study to estimate water seepage from northwestern Lake Nasser, Egypt. *Journal of Geophysics and Engineering*, 3(1), 21–27. <https://doi.org/10.1088/1742-2132/3/1/003>
- Nazoumou Y (2002) Impact des barrages sur la recharge des nappes en zone aride: étude par modélisation numérique sur le cas de Kairouan (Tunisie centrale) (Doctoral dissertation, Université de Tunis El Manar).
- Ozer A, Paskoff R, Sanlaville P, Ulzega A (1980) Essai de corrélation du Pléistocène supérieur de la Sardaigne et de la Tunisie. *Comptes Rendus Hebdomadaires des Séances de l'Académie des Sciences. Série D, Sciences Naturelles*, 291, 801-804.
- Paniconi C, Khlaifi I, Lecca G, Giacomelli A, Tarhouni J (2001) Modeling and analysis of seawater intrusion in the coastal aquifer of Eastern Cap-Bon, Tunisia. *Transport in Porous Media*, 43(1), 3–28. <https://doi.org/10.1023/a:1010600921912>
- Panthulu T V, Krishnaiah C, Shirke J M (2001) Detection of seepage paths in earth dams using self-potential and electrical resistivity methods. *Engineering Geology*, 59(3-4), 281-295.
- Samouëlian A, Cousin I, Tabbagh A, Bruand A, Richard G (2005) Electrical resistivity survey in soil science: A review. *Soil and Tillage Research*, 83(2), 173–193. <https://doi.org/10.1016/j.still.2004.10.004>
- Sasaki K (1992) Two new and two resurrected species of the sciaenid genus *Johnius* (*Johnius*) from the West Pacific. *Jap J Ichthyol* 39(3):191–199
- Schmadel N M, Neilson B T, Kasahara T (2014) Deducing the spatial variability of exchange within a longitudinal channel water balance. *Hydrological Processes*, 28(7), 3088–3103. <https://doi.org/10.1002/hyp.9854>
- Sevil J, Gutiérrez F, Zarroca M, Desir G, Carbonel D, Guerrero J, Fabregat I (2017) Sinkhole investigation in an urban area by trenching in combination with GPR, ERT and high-

- precision leveling. Mantled evaporite karst of Zaragoza city, NE Spain. *Engineering Geology*, 231, 9–20. <https://doi.org/10.1016/j.enggeo.2017.10.009>
- Simmers I (1998) Groundwater recharge: An overview of estimation ‘problems’ and recent developments. *Geological Society, London, Special Publications*, 130(1), 107–115. <https://doi.org/10.1144/gsl.sp.1998.130.01.10>
- Somers L D, Gordon R P, McKenzie J M, Lautz L K, Wigmore O, Glose A, Condom T (2016) Quantifying groundwater–surface water interactions in a proglacial valley, Cordillera Blanca, Peru. *Hydrological Processes*, 30(17), 2915–2929. <https://doi.org/10.1002/hyp.10912>
- Temani, R, Nachite D, Sciuto F, Razgallah S, Bekkali R, Hayet K, Gaaloul N (2016) Les Ostracodes plio-pléistocènes des séries sédimentaires de la bordure orientale du Cap Bon (coupe de l'Oued Lebna, Tunisie orientale). *Carnets de Géologie*, 16(18), 431–447. <https://doi.org/10.4267/2042/61387>
- Thornthwaite C W, Mather J R (1957) Instructions and tables for computing potential evapotranspiration and the water balance. Centerton.
- Yi P, Yang J, Wang Y, Mugwanezal V, Chen L, Aldahan, A. (2018) Detecting the leakage source of a reservoir using isotopes. *Journal of Environmental Radioactivity*, 187, 106–114. <https://doi.org/10.1016/j.jenvrad.2018.01.023>
- Zghibi A, Merzougui A, Zouhri L, Tarhouni J (2014) Understanding groundwater chemistry using multivariate statistics techniques to the study of contamination in the Korba unconfined aquifer system of Cap-Bon (North-east of Tunisia). *Journal of African Earth Sciences*, 89, 1–15. <https://doi.org/10.1016/j.jafrearsci.2013.09.004>
- Zghibi A, Tarhouni J, Zouhri L (2013) Assessment of seawater intrusion and nitrate contamination on the groundwater quality in the Korba coastal plain of Cap-Bon

- (North-east of Tunisia). *Journal of African Earth Sciences*, 87, 1–12.
<https://doi.org/10.1016/j.jafrearsci.2013.07.009>
- Zghibi A, Zouhri L, Tarhouni J (2011) Groundwater modelling and marine intrusion in the semi-arid systems (Cap-Bon, Tunisia). *Hydrological Processes*, 25(11), 1822–1836.
<https://doi.org/10.1002/hyp.7948>
- Zhang D, Han D, Song X (2020) Impacts of the sanmenxia dam on the interaction between surface water and ground water in the Lower Weihe River of Yellow River Watershed. *Water*, 12(6), 1671. <https://doi.org/10.3390/w12061671>
- Zhao T, Richards, K S, Xu H, Meng H. (2012) Interactions between dam-regulated river flow and riparian groundwater: A case study from the Yellow River, China. *Hydrological Processes*, 26(10), 1552–1560. <https://doi.org/10.1002/hyp.8260>
- Zhou Z, Zhou Z, Xu H, Li M (2021) Surface water–groundwater interactions of Xiluodu Reservoir based on the dynamic evolution of seepage, temperature, and hydrochemistry due to impoundment. *Hydrological Processes*, 35(8), e14304.
<https://doi.org/10.1002/hyp.14304>
- Ziadi A, Hariga N. T, Tarhouni J (2017) Use of time-domain electromagnetic (TDEM) method to investigate seawater intrusion in the Lebna coastal aquifer of eastern Cap Bon, Tunisia. *Arabian Journal of Geosciences*, 10(22), 492.
<https://doi.org/10.1007/s12517-017-3265-9>
- Ziadi A, Hariga N T, Tarhouni J (2019) Mineralization and pollution sources in the coastal aquifer of Lebna, Cap Bon, Tunisia. *Journal of African Earth Sciences*, 151, 391–402.
<https://doi.org/10.1016/j.jafrearsci.2019.01.004>

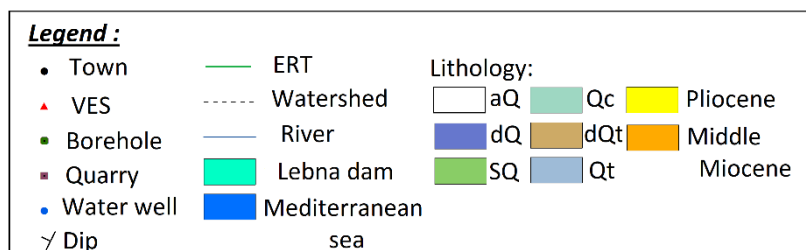
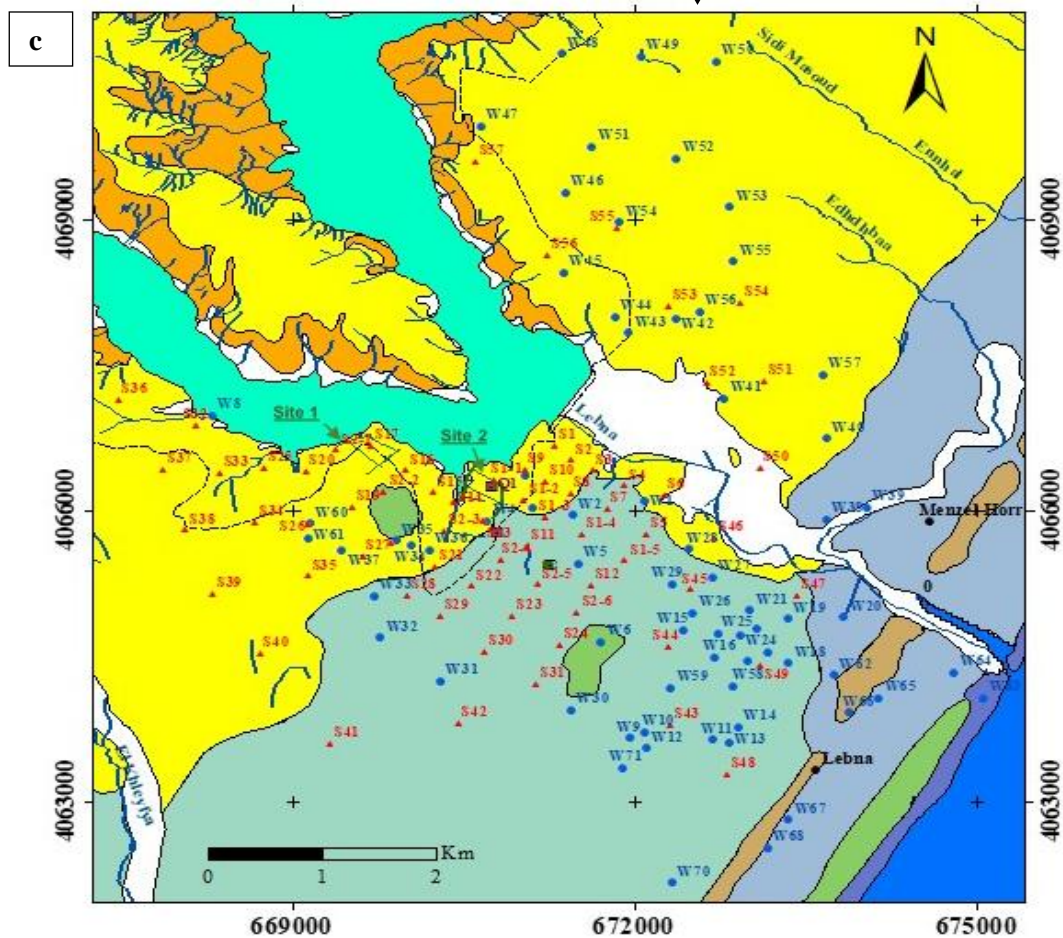
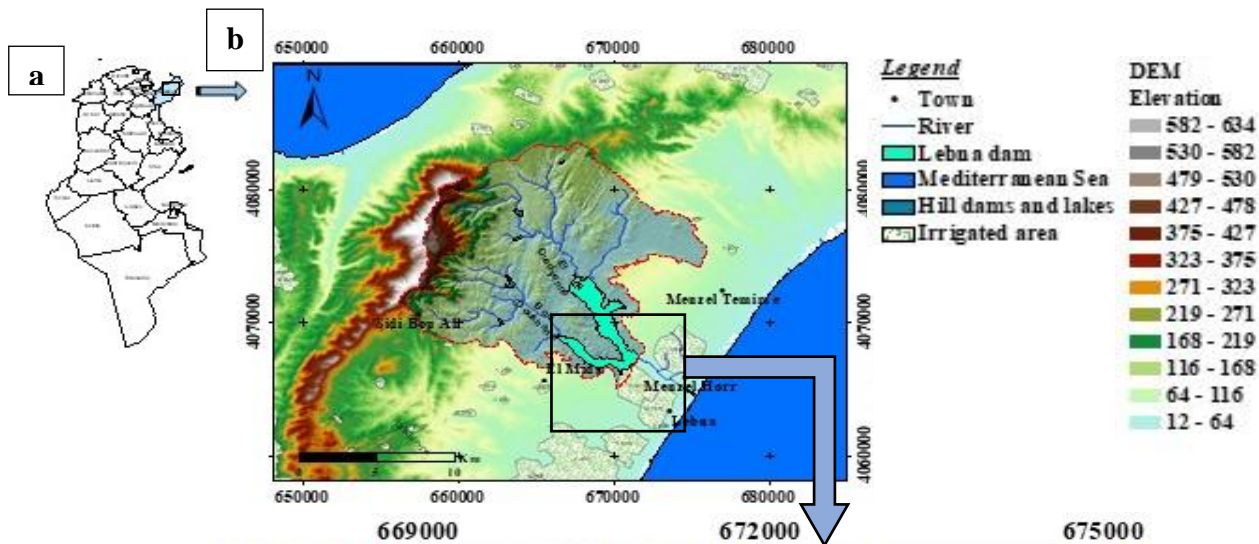


Figure 1: Location and geologic map of the study area. (1) Tunisian map; (b) geographical situation and digital terrain model of the Lebna watershed relative to the Cap Bon peninsula and to the country of Tunisia; (c) geological setting based on maps (Sheet N° 22: Realized by M. Arnould (1951), actualized by H. Ben salem (1997) and Sheet N° 15: by Bensalem 1997), with well-sampled, borehole, quarry and VES locations; and (c) ERT profile locations.

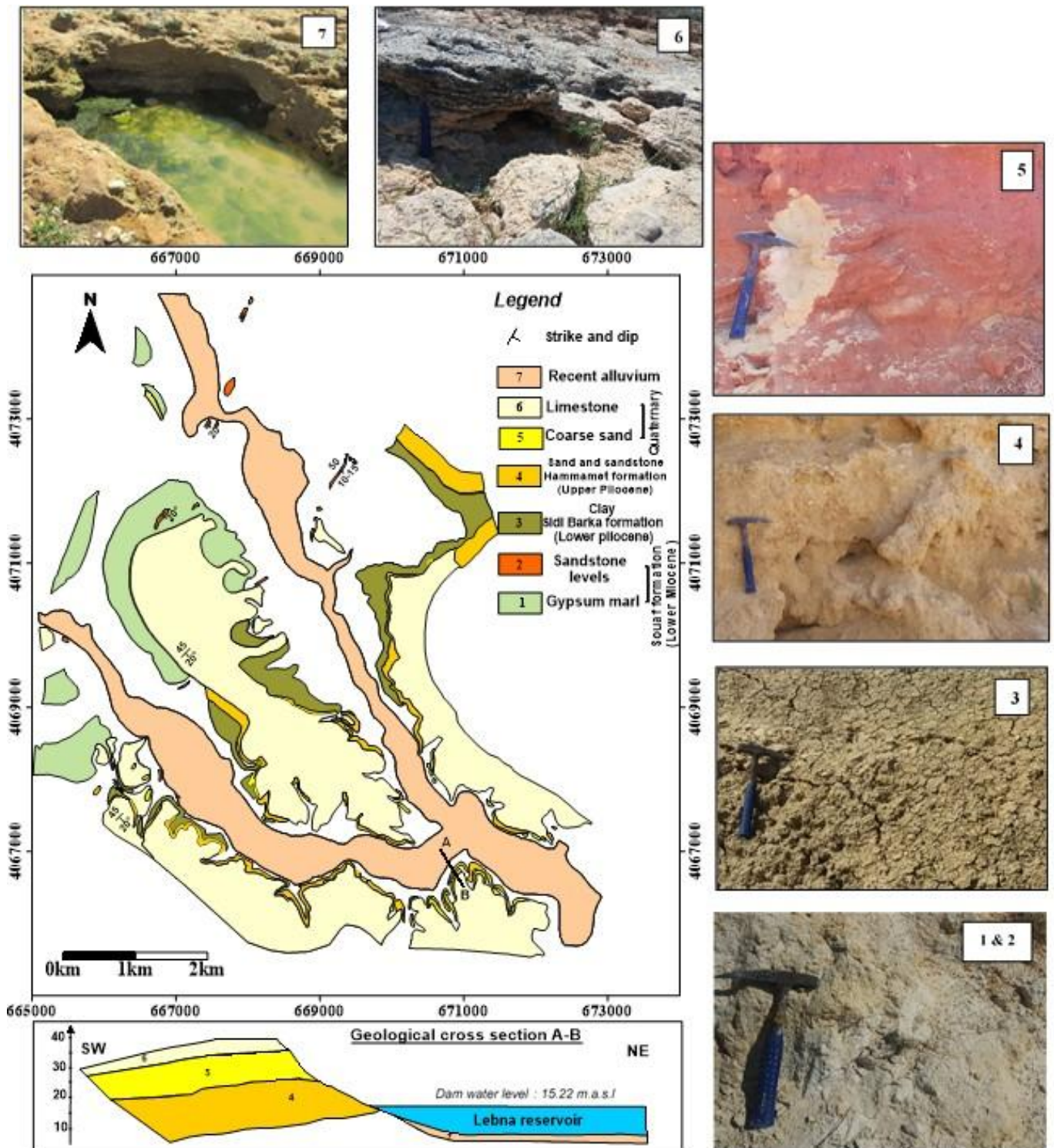


Figure 2: Geological map of the Lebna Dam basin, illustrated by pictures captured in 2019 depicting the sedimentology and nature of outcropping units in the study area and the AB cross section realized in the downstream region of the Lebna Basin.

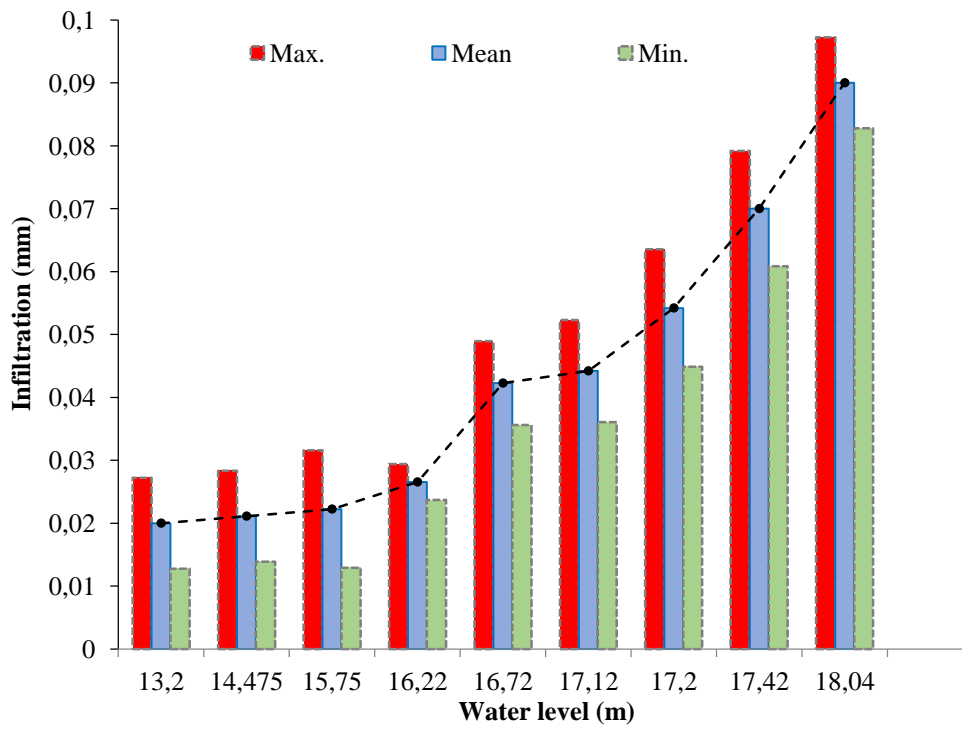


Figure 3: Infiltration from the Lebna reservoir as a function of the water level.

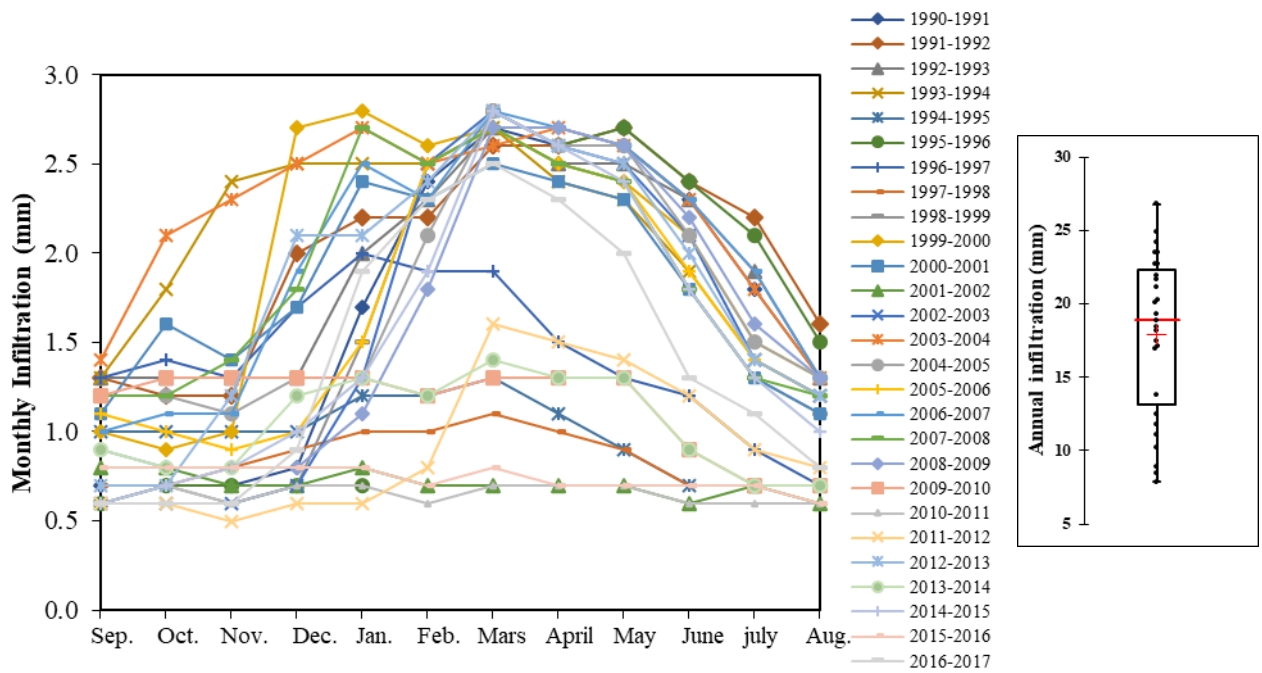


Figure 4: Average monthly infiltration rate from the Lebna Dam reservoir over 27 years (1990-2017).



Figure 5: Schematic illustration of the water balance terms of the Lebna Dam.

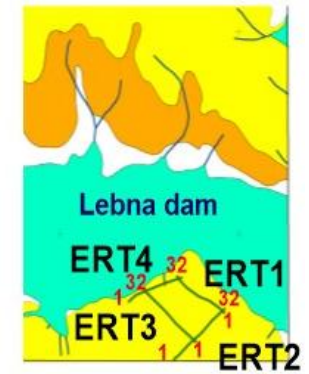
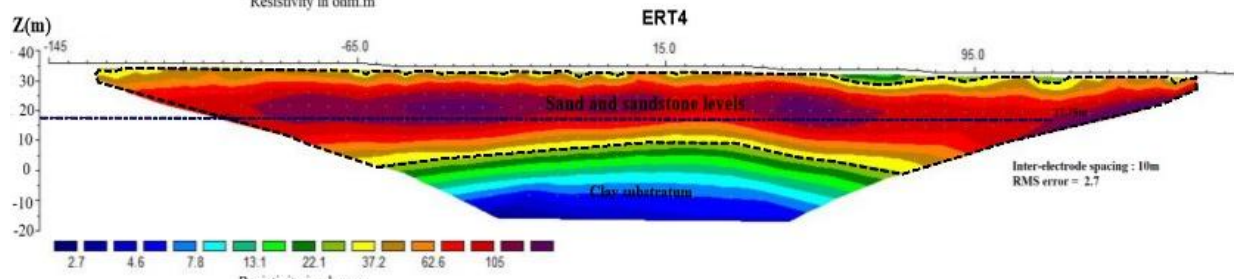
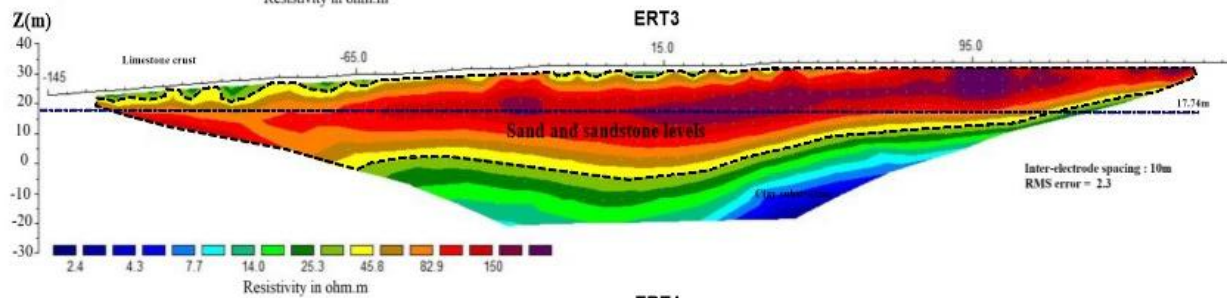
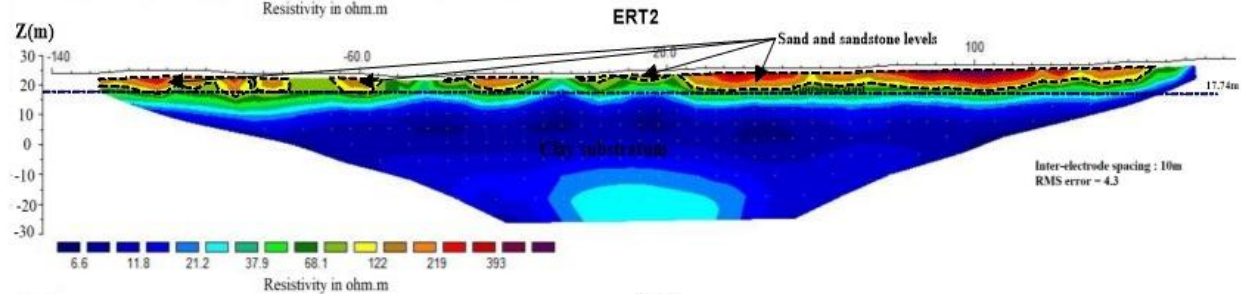
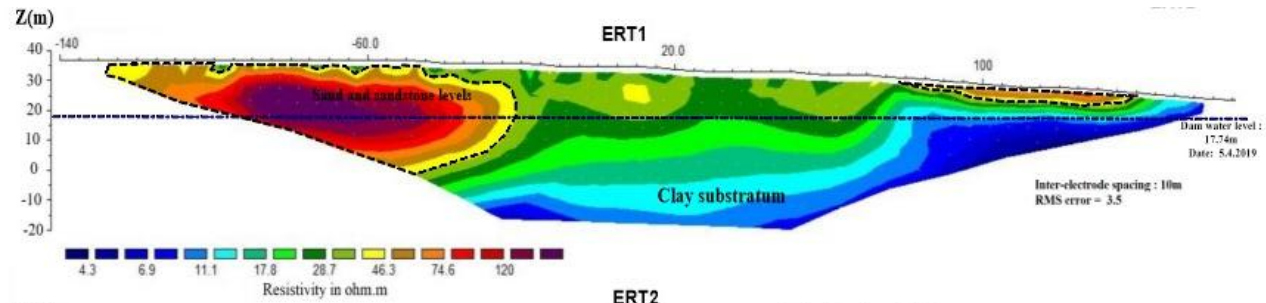


Figure 6: Resistivity models of site 1 including the topography derived by the ERT method and the Wenner array of site 1.

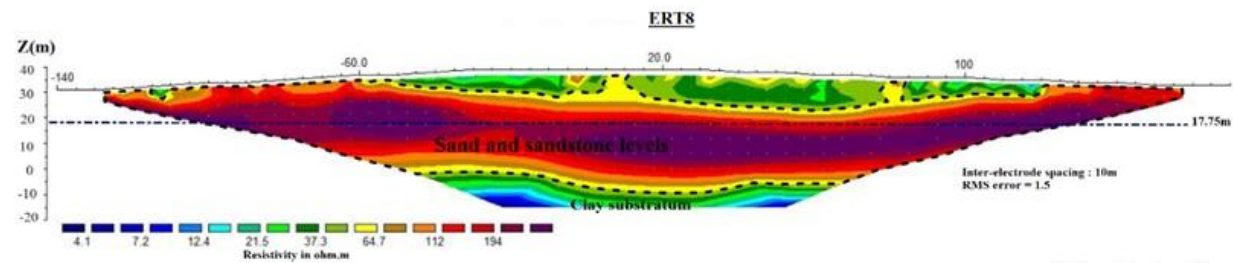
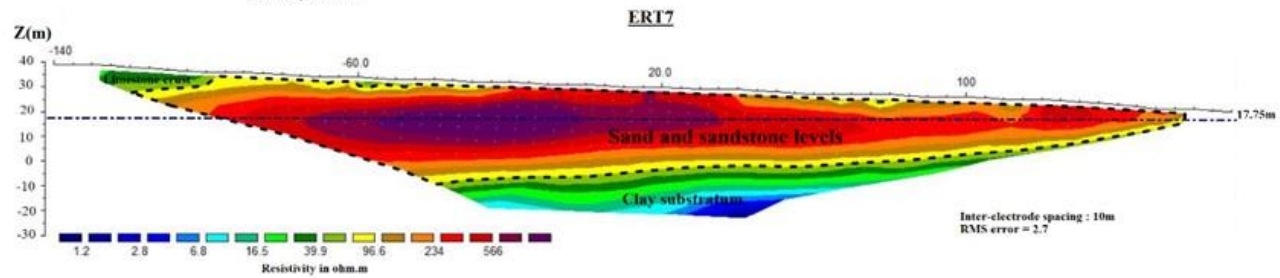
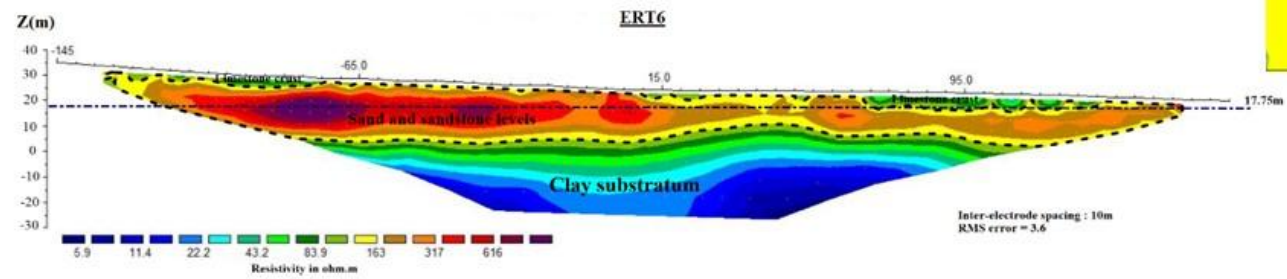
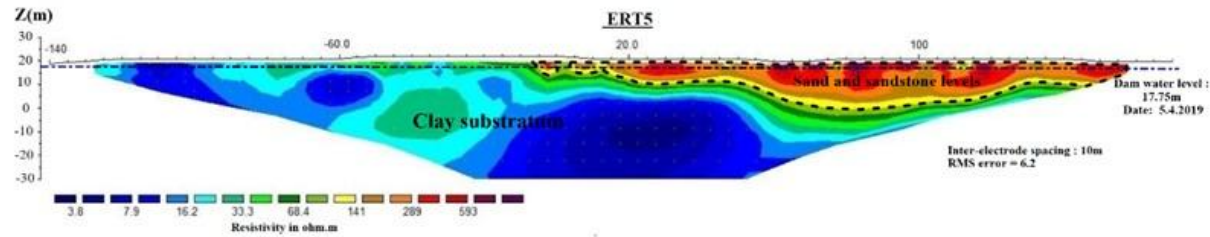
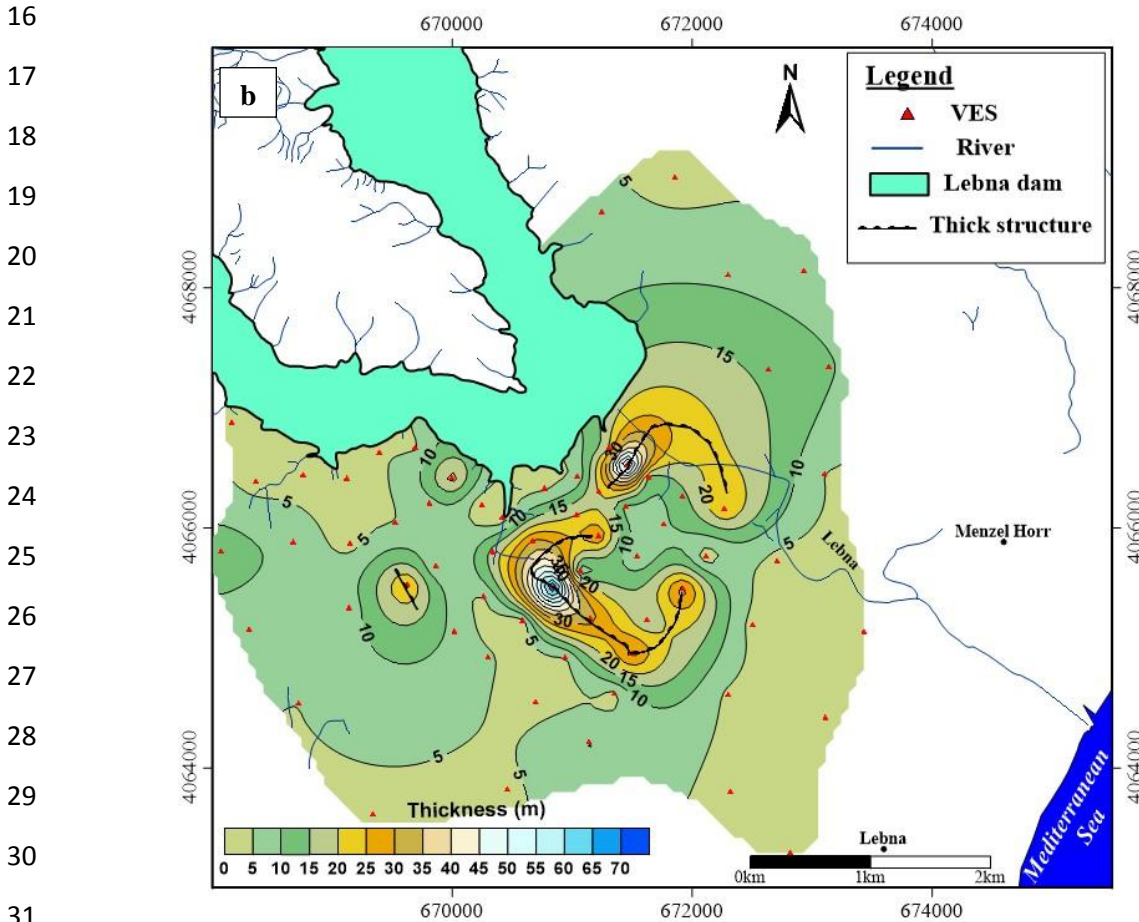
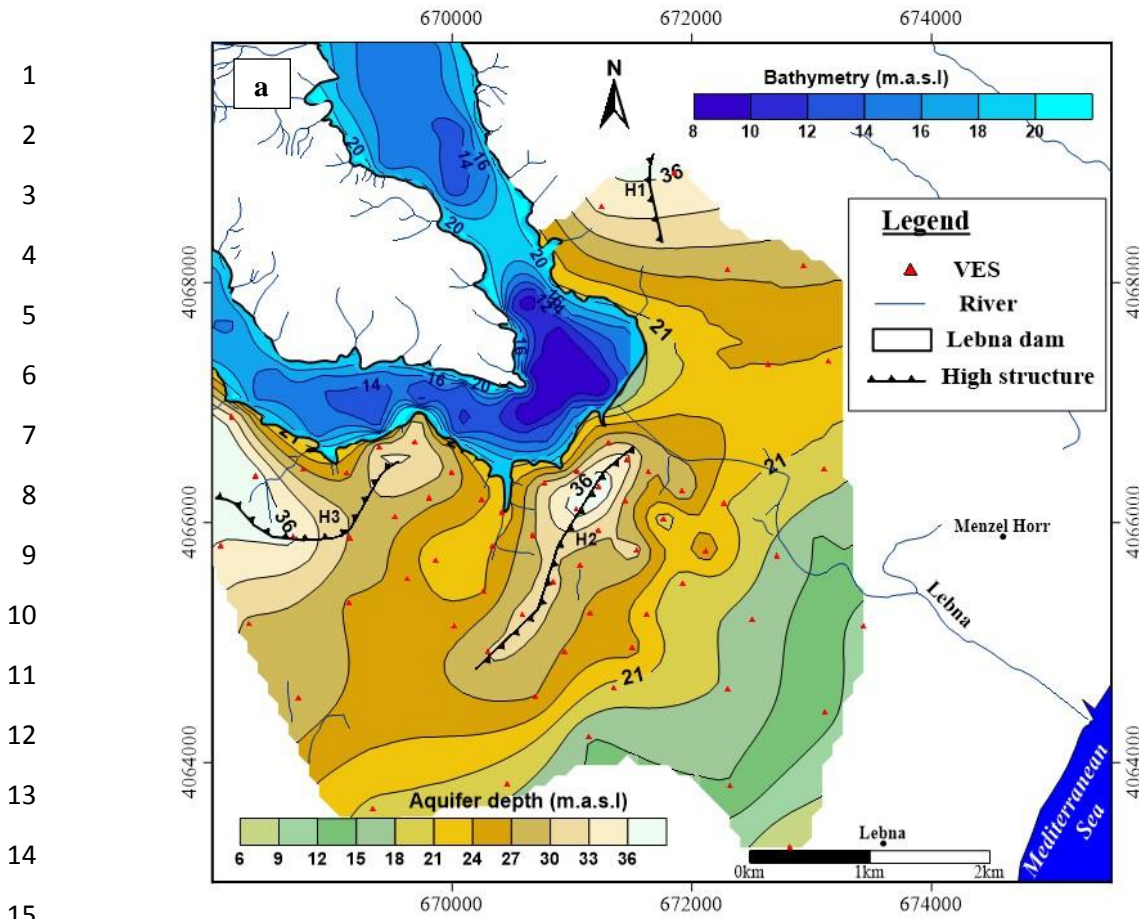


Figure 7: Resistivity models including topography obtained using the Wenner ERT method of site 2.



44
Figure 8: (a) Isobath map and (b) isopach maps of the Lebna Basin shallow aquifer.

32
33
34
35
36
37
38
39
40
41
42
43
44
45
46
47
48
49
50
51
52
53
54
55
56
57
58
59
60
61
62

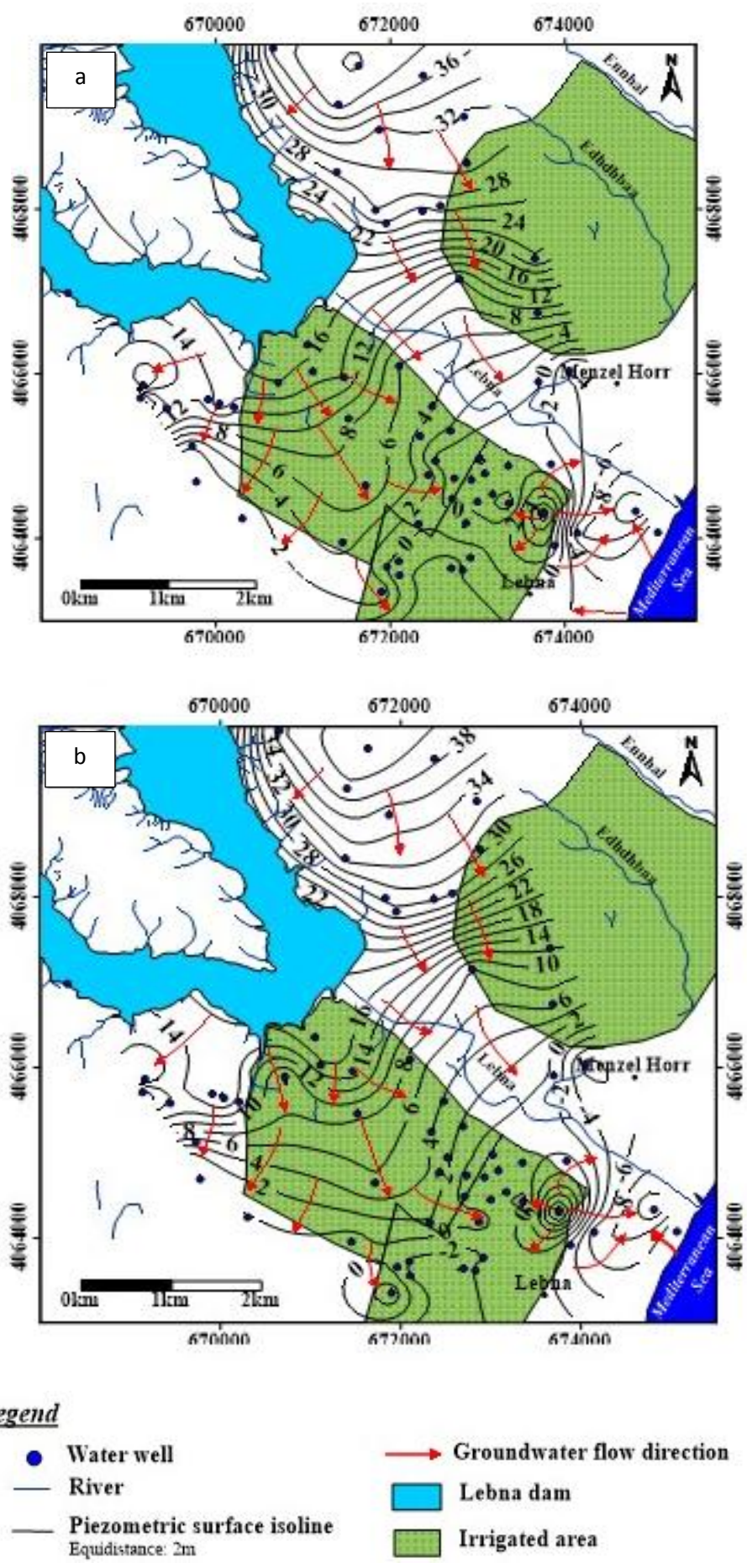
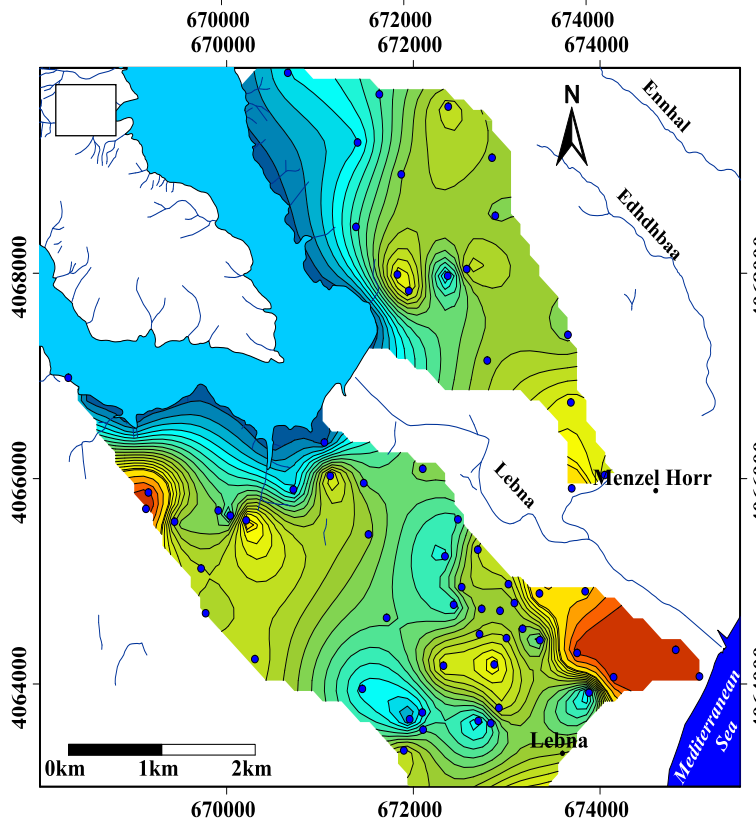
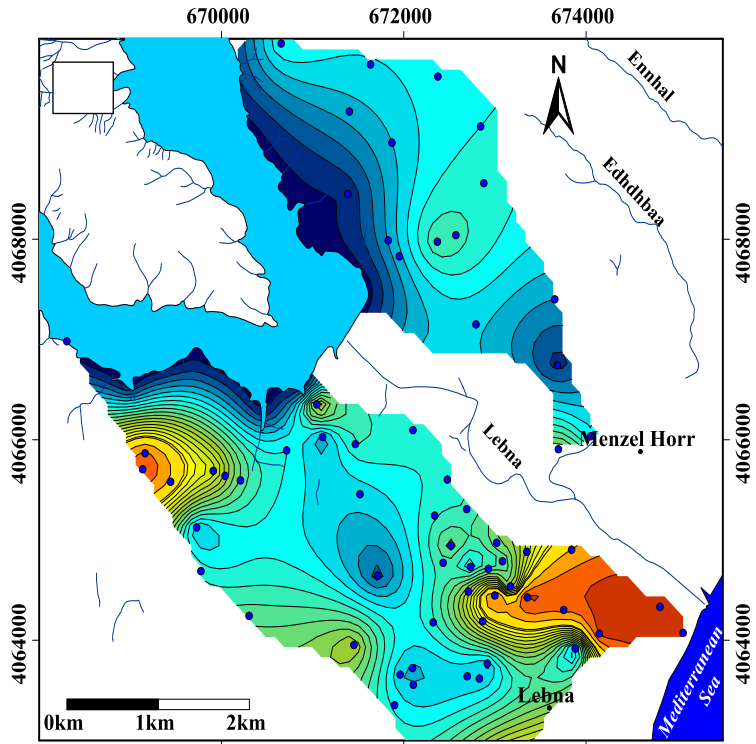


Figure 9: Piezometric maps of the coastal aquifer: (a) in February 2019; (b) in August 2019.

63

64



65

66

67

Legend

- Water well
- River
- Lebna dam



68

69

70 **Figure 10:** Spatial distributions of groundwater electrical conductivity (mS/cm) in the Korba
71 Basin aquifer: (a) February 2020; and (b) August 2020.

72

73 **TABLES**

74

75 **Table 1.** Annual classification according to the water level interval (measured during the dry
76 season)

Group:	1	2	3	4	5	6	7	8
Interval in m [from-to]:	[17.5-18]	[16.5-17.8]	[16.5-17.7]	[15.9-17.1]	[15.2-16.8]	[15-16.5]	[14-15.7]	[13.2-15.3]
			1993					
	1991		1994					
	1992	2003	1999					
Years :	1996	2011	2000	2013	2010	1995		2002
	2004	2015	2001	1997	2014	1998	2017	2012
	2007	2016	2005					
	2009		2006					
			2008					

77

78

79
80
81
82
83
84
85
86
87
88
89
90
91
92
93
94
95
96
97
98

Supplementary materials

Title: Geophysical and Hydrogeological Investigations of Water Leakage from a Reservoir Dam to a Coastal Aquifer: The Lebna Case Study (Northeastern Tunisia)

Journal: Arabian journal of Geosciences

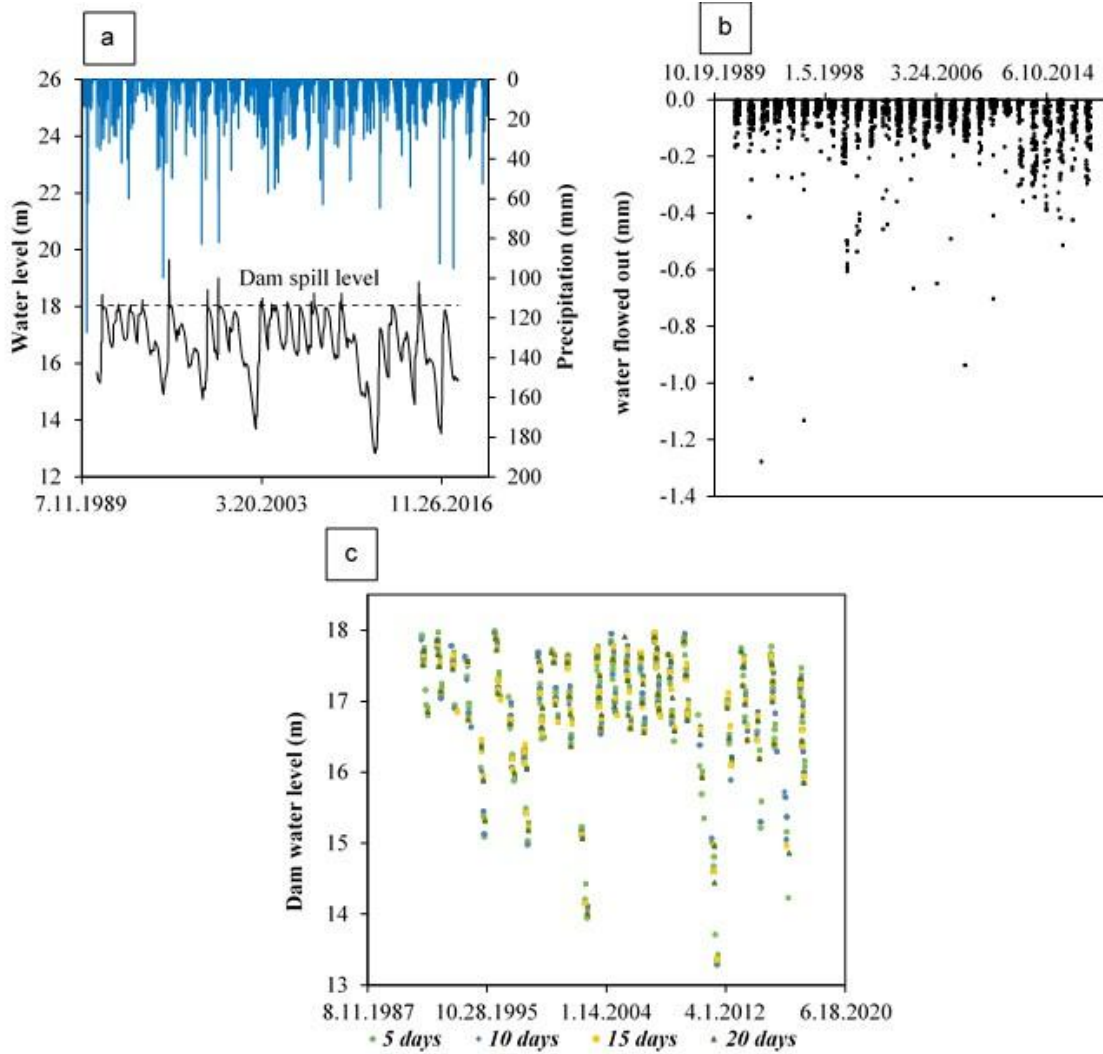
Authors: Nejmeddine Ouhich ^{1,2,3,*}, Radhouane Hamdi ³, Fethi Lachaal ¹, Hakim Gabtni ¹, and Olivier Grunberger³

¹ LGR/LR15 WRTC 01, CERTE, Borj Cedria Ecopark, Soliman, Tunisia

² FST, Campus Universities, El Manar, Tunis, Tunisia

³ Univ Montpellier, INRAE, IRD, Institut d'Agro, UMR LISAH, Montpellier, France

Corresponding Author: nejmeddinouhichi@gmail.com



99

100 **ESM_1** : Dam water balance feature analysis: (a) rainfall and water level time series in the
 101 dam; (b) water balance calculated in the dry season; and (c) reservoir water level evolution
 102 during the dry season, denoting the groups of years classified by dam water level ranges.

103

104

105

106

107

108

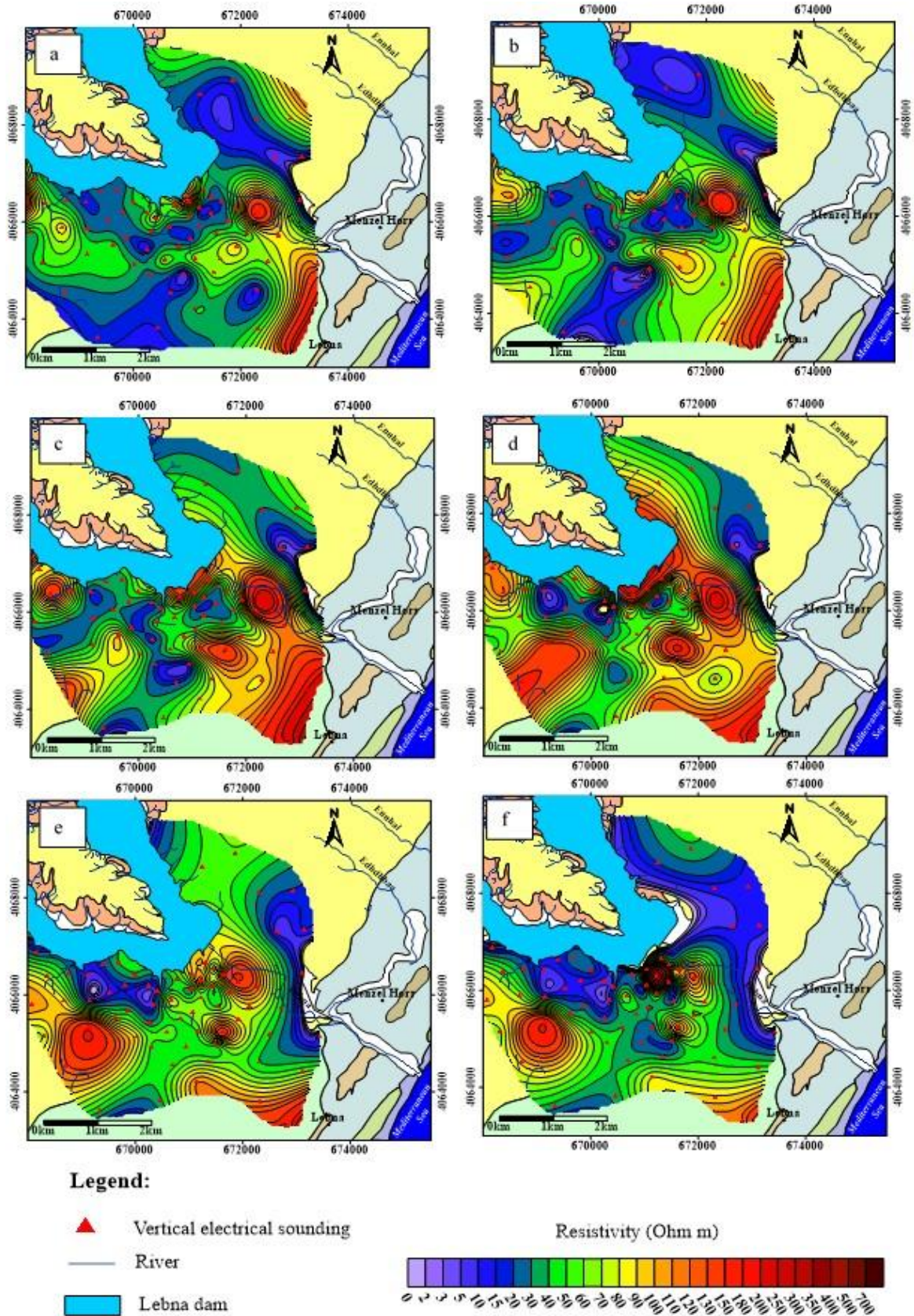
109

110

111

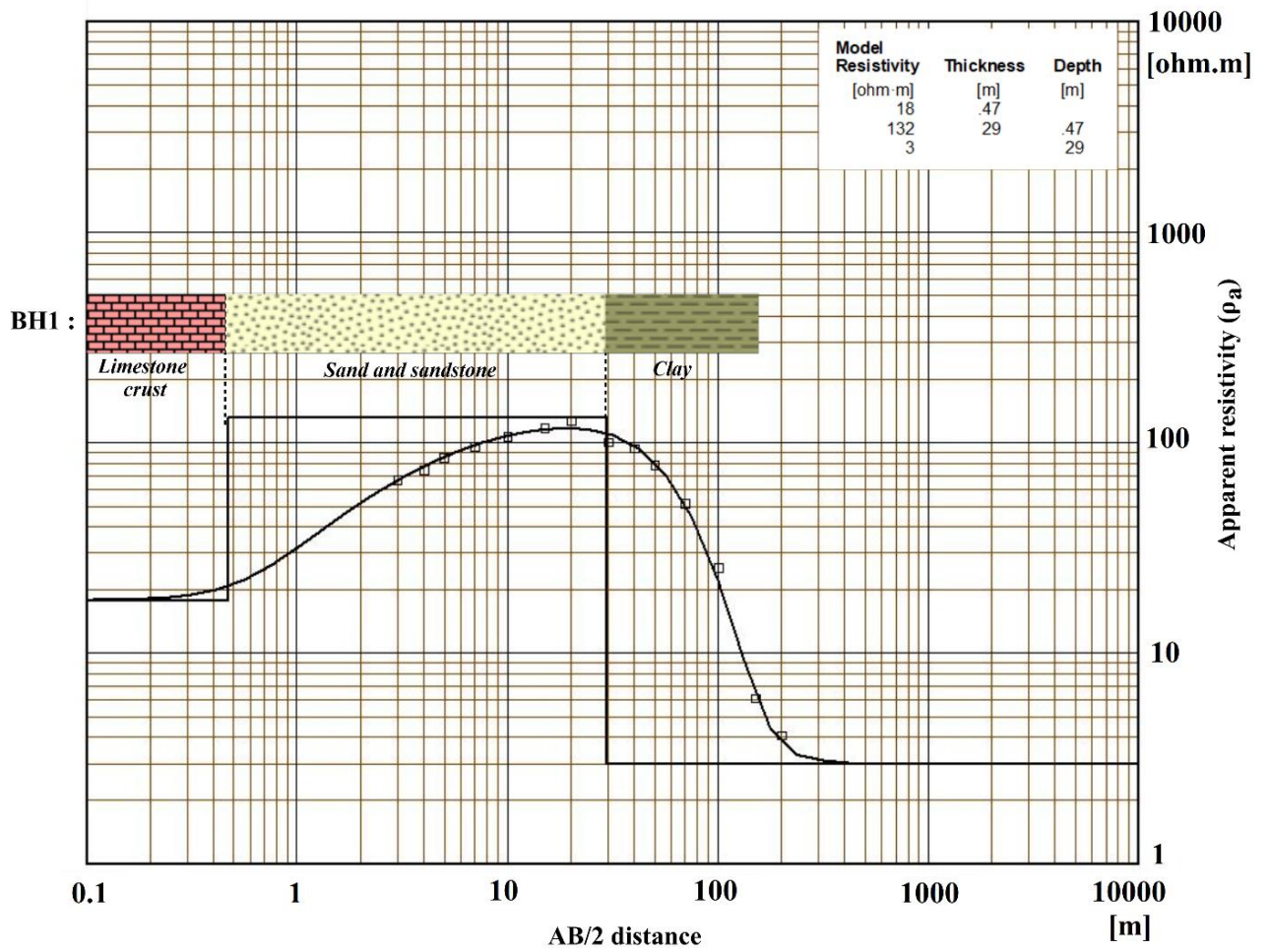
112

113



114

115 **ESM_2:** Isoapparent resistivity map of the subsoil: (a) $AB/2 = 3$ m; (b) $AB/2 = 7$ m; (c)
 116 $AB/2 = 15$ m; (d) $AB/2 = 30$ m; (e) $AB/2 = 70$ m; and (f) $AB/2 = 100$ m.

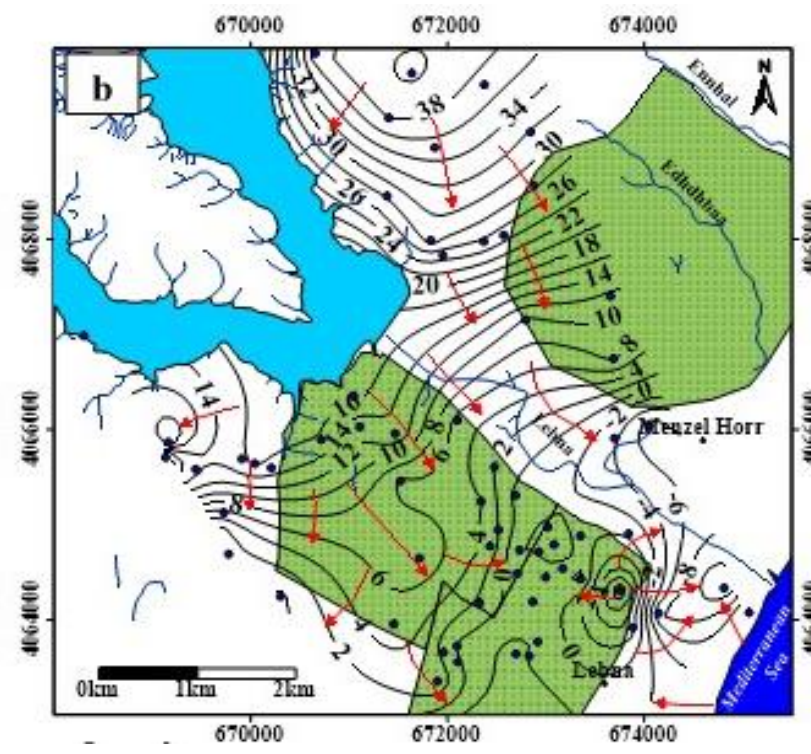
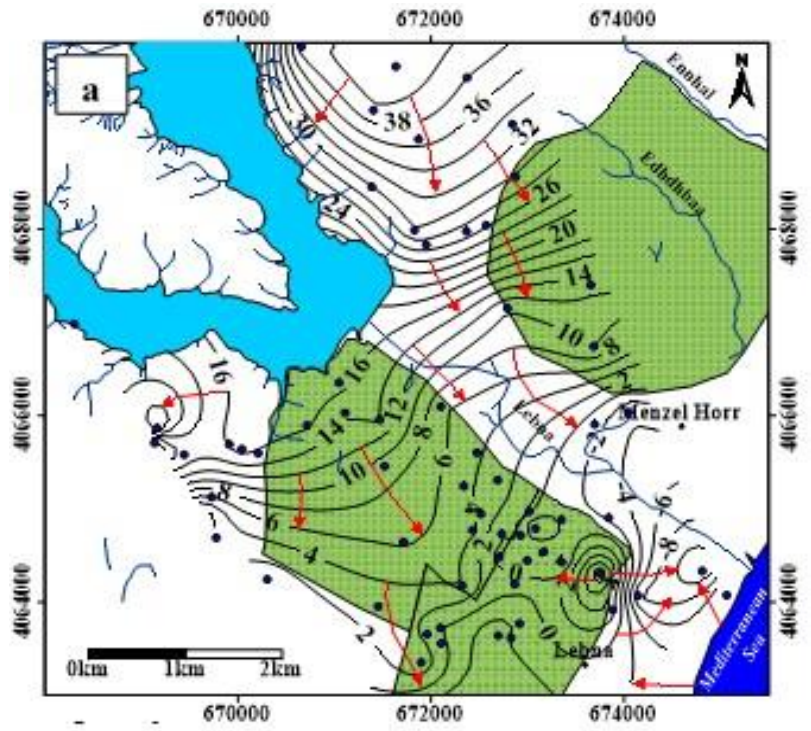


117

118

ESM_3: Calibration of the S2-5 VES with the BH1 borehole

119



Legend

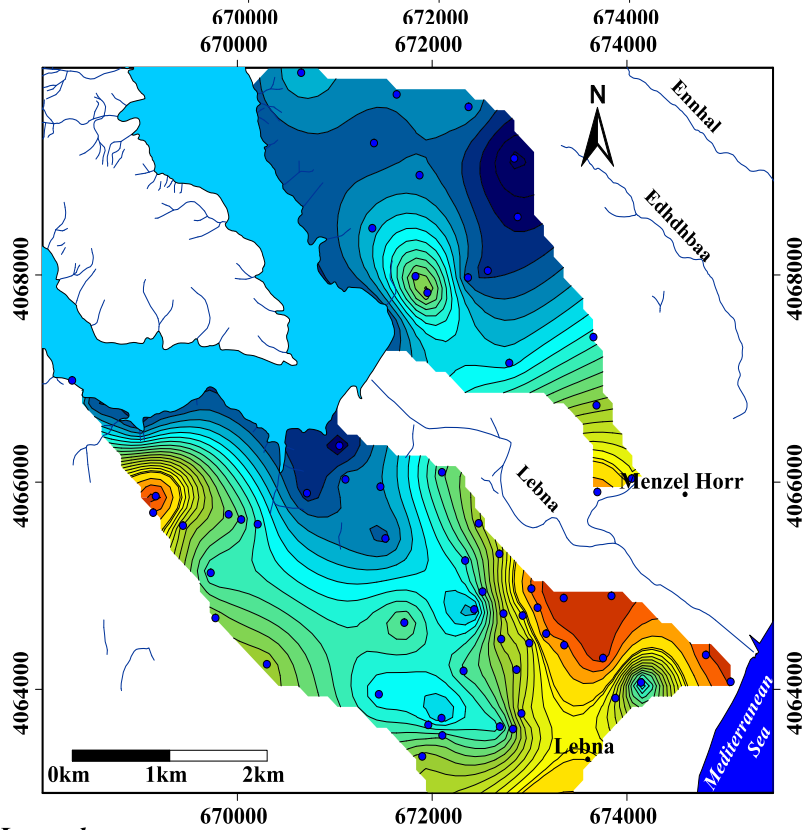
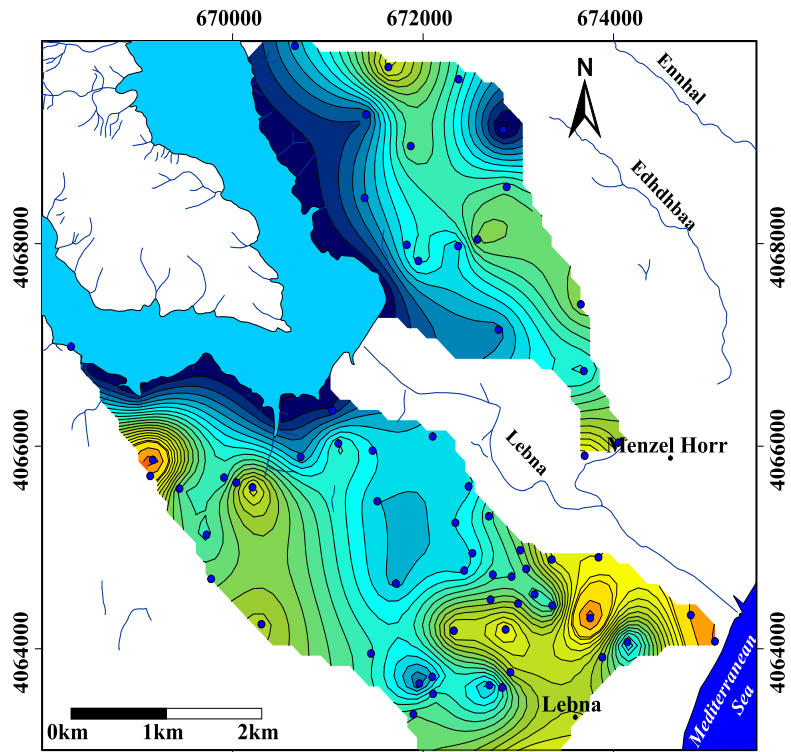
- Water well
- River
- Piezometric surface isoline
Equidistance: 2m
- Groundwater flow direction
- Lebna dam
- Irrigated area

120

125

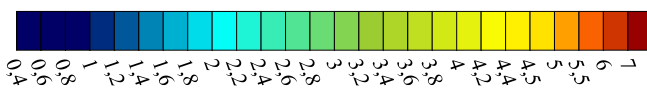
126

ESM_4: Piezometric maps of the coastal aquifer: (a) in February 2019; (b) in August 2019.



Legend

- Water well
- River
- Lebna dam



127

128

129

ESM_5: Spatial distributions of groundwater electrical conductivity (mS/cm) in the Korba Basin aquifer: (a) February 2019; and (b) August 2019.

